æ

9. CELL GROWTH AND DIVISION

29 November 2020

The central mission of all cells – to survive and reproduce – is a product of the relentless operation of natural selection. For unicellular organisms, the matter of cellular reproduction naturally also brings us into contact with the issue of cellular growth. Typically, cells reproduce by binary fission, although there are cases in which offspring and adult cell sizes differ by more than two-fold, e.g., budding in some yeast, and multiple internal fissions in some algae. The essential issue is that continuous proliferation of a population requires the growth of individual cells. Growth, in turn, requires the intake and conversion of nutrients to biomolecules.

Here, we focus on the general challenges that exist for any growth mechanism, leaving the molecular details on resource uptake and cell division to subsequent chapters (10 and 18, respectively). First, cell growth requires coordination between the intake of resources and their conversion into cellular material, mostly proteins, nucleic acids, and lipids. Even the simplest of cells consist of thousands of types of molecules, so the overall process is enormously complex. The question here is whether the degree to which the basic process of cell growth can be understood in general terms using models incorporating a minimum level of molecular complexity.

Second, in relating growth in cellular biomass to the matter of cell division, the primary question is how a cell decides when to multiply. In principle, cells might simply divide after a critical time period has passed, although this would require slowing the clock down in nutrient-poor environments. Alternatively, division might be delayed until a critical cell size, possibly environmentally determined, is reached. Still another possibility is that the license to divide is based on the attainment of a specific growth increment, in which case the size at division would be defined by the prior size at birth. Regardless of the target criterion, cells must generally possess compensatory mechanisms to prevent runaway growth or diminution in size in extreme individuals.

Third, cell division is not a perfect process. There is always some size variation among the sister cells resulting from binary fission, and this inevitably leads to variance in the partitioning of the parental-cell contents. Resulting entirely from the limits to the perfection of cell-division mechanisms, such variation generates phenotypic variation even in otherwise genetically uniform populations, and at a level much higher than observed in multicellular species. Some have argued that the production of phenotypic variation has been promoted by natural selection as a bet-hedging strategy to cope with heterogeneous environments. However, as discussed below, nongenetic sources of phenotypic variation reduce the efficiency of natural selection and impose long-term fitness loads, leaving many open questions on this matter.

Ribosomes and Cell Growth

Before considering the more quantitative aspects of growth, an overview of some relevant issues regarding the molecular machine dedicated to protein production is in order. Cells make enormous investments in ribosomes, with up to 50% of all transcription being devoted to the production of ribosomal RNA (the catalytic heart of the ribosome) and up to 50% of messenger RNA production allocated to the production of ribosomal proteins (Warner et al. 2001). Given that each ribosome can process only one mRNA at a time, and that ribosomes are energetically expensive to produce, one might expect a strong regulatory associations between cellular growth rates and the number of ribosomes per cell. Overly low numbers of ribosomes relative to the cellular supply of nutrients would compromise the rate of production of cellular biomass. However, excess investment in ribosomes would divert energy from other cellular processes essential to resource acquisition. This simple argument suggests that there should be some sort of developmental scaling between the number of ribosomes per cell and the cellular growth rate (Foundations 9.1).

Consistent with this expectation, for all species in which the issue has been addressed, there is a strong and essentially linear relationship between cell growth rate and the mass ratio of total RNA to total protein in the cell (Figure 9.1A). In other words, there is a predictable shift in the molecular contents of cells as they are exposed to more nutrient-enriched environments. Generally, the RNA/protein ratio is in the range of 0.1 to 0.2 at low growth rates, and then increases to ∼0.5 or even more in the fastest growing cells. These types of responses are retained even when the growth-rate differences are created by varying the types of substrates (as opposed to altering the concentration of a single limiting nutrient) (Schaechter et al. 1958; Fraenkel and Neidhardt 1961). Thus, the level of RNA production is driven by an indirect regulatory connection with the growth rate itself, rather than by direct resource-specific signals.

Although the patterns illustrated in Figure 9.1A refer to the total RNA in a cell, additional data suggest a coordinated response for mRNAs, tRNAs, and rRNAs, such that the number of ribosomes per cell also scales directly with the cellular growth rate. For most species that have been examined, the ratio of rRNA to total RNA in cells falls in the range of 0.55 to 0.88, typically not deviating by more than 0.15 between different growth rates (Figure 9.1B). Thus, with increasing nutrient availability, the number of ribosomes per cell increases in a coordinated way with the growth rate.

Such proportionality appears to arise from various feedback mechanisms. Ribosome biogenesis is often controlled indirectly by the level of free rRNA in the cell, the production of which is in turn regulated via the amount of uncharged tRNAs (Liu et al. 2015). In *E. coli,* for example, an alarmone (ppGpp) is produced when uncharged tRNAs accumulate in the face of an inadequate supply of amino acids, and this suppresses rRNA production (Potrykus et al. 2011). When ribosomal proteins are in excess in the cell relative to the rRNAs to which they must bind, the former bind to their own mRNAs, thereby repressing their own production. In contrast, in the soil bacterium *Bacillus subtilis*, inhibition of rRNA production results from a drop in cellular GTP levels (a result of enhanced incorporation of GTP into ppGpp) (Krásný and Gourse 2004). A variety of other mechanisms exist in eukaryotes (Warner et al. 2001; Parenteau et al. 2019). Such regulatory flexibility of a highly conserved function will be encountered for a number of other cellular traits in the following pages.

A relatively simple theoretical argument potentially explains the linear response of investment in ribosomes with increasing growth rate (Foundations 9.1). Assuming that all but a small fixed fraction of ribosomes is actively engaged in translation and that active ribosomes are generally saturated with mRNAs, the overall growth rate can only be enhanced by increasing the translation rate per ribosome and/or the number of ribosomes. For species with available data, translation rates per ribosome generally change by no more than a factor of two over a scale in which the cell growth rate varies much more (Figure 9.1C). Thus, elevated investment in ribosomes appears to be the dominant factor.

Under this view, a plot of the mass ratio of ribosomal protein to total protein against the cell growth rate (Equation 9.1.3) has a specific biological meaning – the y intercept is a measure of the investment in inactive ribosomes relative to the total pool of proteins, and the inverse of the slope is a measure of the rate of protein mass produced per mass of ribosomal protein. Figure 9.1A provides such a plot for *E. coli,* except that the y-axis values need to be multiplied by 0.53 to convert to the ribosomal protein ratio for this species (Scott et al. 2010). Although *E. coli* will be used as an exemplar in the following analyses, this species has a distinctly lower intercept and slope for the response plot than in other species, meaning that *E. coli* achieves a maximum growth rate with a relatively low investment in RNA (and presumably ribosomes).

The total investment in ribosomal proteins in *E. coli* can be obtained by multiplying the total RNA/total protein mass ratio by the average rRNA/total RNA ratio of 0.62 from Dennis and Bremer (1974), and then by the ratio of ribosomal protein to rRNA mass of 0.53. From Figure 9.1A, this leads to the conclusion that $\sim 3\%$ of the protein in a nongrowing *E. coli* cell is associated with ribosomes. This is in reasonable agreement with a more direct estimate of $\sim 8\%$ associated with nontranslating ribosomes in budding yeast, regardless of the growth rate (Metzl-Raz et al. 2017). Although ribosomes are expensive to produce, a non-zero reserve at near-zero growth rate is not too surprising, as complete ribosome loss is a death sentence. Although little work has been done on the matter, in *E. coli* and likely other bacteria, ribosomes dimerize and become translationally quiescent under nutritionally starved states (Vila-Sanjurjo 2008; Yoshida and Wada 2014).

The fractional investment in ribosomal proteins increases to 28% for cells growing at maximum rate, and Scott et al. (2010) estimate that when the total amount of accessory proteins associated with translation is added in, these numbers need to be multiplied by ~ 1.7 to determine the total investment in translation. Thus, a rapidly growing *E. coli* cell devotes nearly 50% of its protein to translation. Although the data are less extensive, because eukaryotes have both higher total RNA/total protein and rRNA/total RNA mass ratios than bacteria (Figure 9.1A,B), as well as higher numbers of ribosomal proteins per ribosome (Chapter 6), to achieve equivalent growth rates eukaryotic cells must make an even larger fractional investment in ribosome production.

The results in Figure 9.1 can also be used to estimate the absolute upper bound on the growth rate, by considering the division time of a hypothetical cell consisting entirely of ribosomes. The inverse of the slope in Figure 9.1A implies a rate of protein mass produced per unit ribosome mass per hour of 7.5, indicating that a healthy *E. coli* ribosome can replace its own protein constituents in about $60/7.5 = 8$ minutes. The upper limit to the growth rate can also be calculated more directly by simply considering the number of amino acids per ribosome and the upper bound to the rate of translation (again, assuming that the cell consists of nothing but actively engaged ribosomes). The full set of bacterial ribosomal proteins comprises $\sim 7,500$ amino acids, and the upper bound to the translation rate is ~ 20 amino acids/ribosome/second (Figure 9.1C). If one then liberally assumes that an extended ribosome (the complete translational machinery) contains twice as many amino acids as the ribosome itself, then the rate of addition of amino acids to elongated chains (protein biomass production) per amino-acid residue in the translational apparatus is $20/(2 \cdot 7500) = 0.0013$/second, or 4.8/hour.

Thus, without an increase in the rate of translation or a decrease in the size of an extended ribosome, the cell-division time in an *E. coli*-like bacterium cannot be reduced below ~ 12.5 minutes, indicating that the massive cost of the ribosome itself imposes a significant limit on the rate of cell division. Under optimal growth conditions, many bacteria have doubling times on the order of 20 minutes (Chapter 8), and so are quite close to this ultimate limit.

Models for Cellular Growth

Natural selection promotes phenotypes that maximize the rate of entry of progeny into the subsequent generation, which requires both reproduction and survival. Here, we consider the issues in a very general sense, with an initial focus on simple expressions for the response of cell-division rates to the concentration of a limiting nutrient, e.g., glucose for a laboratory-grown bacterium, or phosphorus for a planktonic alga. This will then be followed by an exploration of how cell size and division time are set and interrelated.

As discussed below, even in a constant environment, substantial variation typically exists in the division times of individual cells, owing to internal stochastic processes. Nonetheless, an ensemble of cells can be described by the average population-level rate of increase r. Letting N_0 and N_t denote population sizes at two points in time, then assuming constant conditions,

$$N_t = N_0 e^{rt} \tag{9.1}$$

describes the trajectory of numbers of individuals over this period (Foundations 9.1). Defined in this way, r is a measure of the per-capita exponential growth rate (with units of time^{-1}). Taking logarithms and rearranging,

$$r = \frac{\ln N_t - \ln N_0}{t}. \tag{9.2}$$

The doubling time for population size, obtained by setting $N_t/N_0 = 2$, is

$$t_d = \ln(2)/r. \tag{9.3}$$

Like interest in a bank account, the doubling time of $\simeq 0.693/r$ is less than expected under linear growth.

The preceding expressions apply to the special situation in which a population is expanding in a nutritionally constant environment, but of course, no population can grow exponentially for an indefinite period of time. In more general applications in population biology, r is usually used to describe the actual rate of population growth, which reflects the net difference between birth and death rates. Here, however, the focus is primarily on laboratory cultures, where there is typically very little cell death. In that case, r can be viewed as the rate of cell birth, which with a constant steady-state distribution of cell sizes at division, is equivalent to the exponential rate of increase in cellular biomass (Jun et al. 2018). In a laboratory culture where cells are being regularly drawn off (as in a chemostat; Figure 8.3), the birth rate can be kept indefinitely at a high level, and it is in this sense that the following descriptions portray the physiological aspects of cellular growth.

From observations on bacteria grown under constant conditions, Monod (1949) concluded that the growth-rate response to nutrient concentration (S) can be described by a simple hyperbolic function,

$$r = r_{\max}\left(\frac{S}{K_r + S}\right), \tag{9.4a}$$

where $r_{\max}$ is the maximum rate of growth (asymptotically approached as $S \to \infty$), and K_r is the half-saturation constant for growth (equivalent to the resource concentration at which $r = r_{\max}/2$). As will be discussed in Chapter 18, this formula is identical in form to the commonly employed Michaelis-Menten equation for nutrient uptake and other enzymatic reactions,

$$u = u_{\max}\left(\frac{S}{K_u + S}\right), \tag{9.4b}$$

where K_u is the half-saturation constant for uptake, which is not necessarily equal to K_r.

Numerous other models have been suggested for linking growth rate to nutrient availability. For example, with a focus on algal cells in continuous culture, Droop (1973, 1974) considered a construct in which the growth rate depends on the *internal* cellular concentration of the limiting nutrient (Q, commonly referred to as the cell quota),

$$r = r_{\max}\left(1 - \frac{\phi}{Q}\right). \tag{9.5}$$

Under this model, cell division ceases when Q drops below the critical internal concentration ϕ, and r asymptotically approaches the maximum possible value $r_{\max}$ as the internal nutritional state Q increases. An attractive feature of this expression is that cell growth is more naturally connected with internal than external nutrient pools. While internal nutrient pools are not necessarily easy to estimate, measures of r and Q in nutrient-limited cultures of single species of phytoplankton have repeatedly supported the general form of Equation 9.5 (Figure 9.2).

Despite its different functional underpinnings, the structure of Equation 9.5 is entirely compatible with the Monod growth equation. This can be seen by noting that for a system in steady-state, the rate of nutrient uptake must equal the product of the cell quota and the rate of cell growth, i.e., $u = r \cdot Q$, which implies a cell quota $Q = u/r$ defined by the ratio of rates of uptake and growth. Substituting this expression into Equation 9.5 and rearranging yields

$$r = r_{\max} \left(\frac{u}{(r_{\max}\phi) + u} \right), \tag{9.6}$$

which again has the form of a hyperbolic relationship, in this case between r and the rate of nutrient uptake. If Equation 9.4b is substituted for u here, a more complex expression is obtained in terms of S and the uptake parameters, but this is still hyperbolic with respect to the external nutrient concentration S, recovering the form of Equation 9.4a.

Equations 9.4a and 9.5 have been used to describe thousands of growth responses, and are often referred to as growth laws. However, the models are phenomenological in the sense that they do not explicitly describe any of the underlying mechanisms connecting substrate uptake, utilization, and growth. They simply describe general growth responses to nutrient limitation with a minimum amount of detail. More complex models have been proposed. For example, Maitra and Dill (2015) and Weiße et al. (2015) presented formulations that include ribosomes, other RNAs, protein, and ATP as the underlying variables, in both cases generating predictions that are consistent with the Monod-growth model and ribosome-growth coupling noted above. Models with an intermediate level of complexity, describing $r_{\max}$ and K_r in mechanistic terms associated with the translational capacity of ribosomes and the nutritional capacity of the environment are outlined in Foundations 9.2. These provide a satisfying explanation for the response to ribosome investment to increased nutrient availability noted in the preceding section.

Control of Cell Size at Maturity

As discussed in the previous chapter, the cell volumes of unicellular species vary by approximately eleven orders of magnitude (Figure 8.1). Within-species deviations exist as a consequence of prevailing environmental conditions, stochastic variation in cell volume arising during division, and position in the cell-division cycle (age variation). Nonetheless, under any particular environmental setting, the range of cell sizes within a species is generally fairly narrow, with standard deviations well below the mean. This implies the existence of homeostatic mechanisms for cell-size regulation.

Under constant conditions, the average rate of increase in cell size (per unit biomass) between divisions must equal the average rate of cell division. If this were not the case, cell size would become progressively smaller or larger. In other words, at steady state, cells must double in size at the same rate as the population doubles in cell number. This, however, leaves open the possibility of a diversity of patterns of biomass growth within the life span of a cell. Resolving this issue is critical to understanding how cell size and division time are jointly determined.

As outlined above, the numbers of cells within populations kept at constant conditions increase exponentially in time (as in a chemostat, where cellular production is continuously offset by removal), and this suggests that the volumes of individual cells might grow in a parallel manner. If so, under steady-state conditions, cell volume would grow in accordance with Equation 9.1,

$$V_t = V_0 e^{rt}, \tag{9.7}$$

where V_0 is the size of a newborn cell, and V_t is its size t time units later. Under this model, the proportional rate of change in cell volume is independent of cell size, although larger cells grow more rapidly in an absolute sense.

Exponential growth specifically implies that the metabolic features of growing cells remain constant, independent of size, such that the ensemble of constituent molecules operates via a fixed set of reaction rates per unit cytoplasmic volume. However, exponential growth in cell size is not essential for balanced growth. The only requirement is that cumulative cellular biomass increases by a factor of two from birth to death. In principle, growth might be linear, with the rate of acquisition of biomass being independent of cell size, or sigmoidal, with the rate of growth initially accelerating and then decelerating as a critical size is approached.

Numerous observations on the growth of individual cells support the exponential cell-growth model (or something very close to it) for bacterial species (Voorn and Koppes 1998; Santi et al. 2013; Iyer-Biswas et al. 2014; Osella et al. 2014; Campos et al. 2014; Susman et al. 2018), with no known striking exceptions. In addition, the model extends to eukaryotes. Godin et al. (2010) and Bryan et al. (2010) observed exponential growth not only in the bacteria *E. coli* and *B. subtilis,* but also in the yeast *S. cerevisiae* and mouse lymphoblast cells, and similar observations have been made on human osteosarcoma cells (Mir et al. 2011) and in the ciliate *Paramecium tetraurelia* (Kimball et al. 1959). In all of these cases, the larger the cell, the higher the absolute growth rate.

In terms of cell-size homeostasis, however, there remains a problem. Owing to stochasticities arising during division, not all cells have exactly the same size at birth. What then regulates the sizes of consecutive cells produced within a lineage to prevent overly small/large cells from spawning ever more extreme descendants? If cells might simply grew exponentially for a specified time before division – a timer model, cells that were larger at birth would grow more over the specified duration, leading to a potentially runaway size distribution (Figure 9.3). Under an alternative sizer model, cells might be programmed to divide once a critical volume is reached.

For the best-studied organism, *E. coli,* both of these models come up short. Instead, for a given environment, cells appear to add an approximately constant volume (Δ) prior to division (Taheri-Araghi et al. 2015) (Figure 9.4). This adder model leads to a simple mechanism of cell-size homeostasis, with the steady-state expected offspring size being equal to Δ. Contrary to the sizer model, the adder model predicts that larger newborn cells will divide at larger sizes (with expectation $V_0 + \Delta$), in effect being oblivious to their current size; only Δ remains independent of size. If a newborn cell is larger than Δ, say by an amount v, then cell division will occur at expected size $(v + \Delta) + \Delta = v + 2\Delta$, and the expected offspring size will be half that, $(v/2) + \Delta$, and hence shifted back towards the long-term expected value Δ by an amount $v/2$. The opposite (a shift towards larger offspring size) occurs if an offspring cell happens to be slightly smaller than Δ. In both cases, the deviations from the expected newborn size decline over time, insuring rapid convergence back to Δ. These arguments ignore new deviations that arise at each subsequent division, and the data suggest that the damping process is less smooth than this simple description implies (Tanouchi et al. 2015), with individual cells having unique response behaviors, presumably reflecting idiosyncratic stochasticies (Susman et al. 2018).

Notably, a pure adder model is not required for cell-size homeostasis. Consider the situation in which there is some memory of parental cell-size (V_p) such that the predicted offspring size is $V_0 = \alpha V_p + \Delta$. Setting $V_0 = V_p$ yields an equilibrium cell size of $\Delta/(1-\alpha)$, which implies homeostasis provided $-1 < \alpha < 1$. If $\alpha < -1$, cell-size declines to zero, and $\alpha > 1$ leads to runaway cell growth, and within the range compatible with homeostasis, positive α leads to faster convergence than negative α.

This more general model accommodates a wide range of species. Like *E. coli,* the one member of the archaea in which the phenomenon has been investigated, *Halobacterium salinarum,* appears to adhere closely to the pure adder model (Eun et al. 2017). However, two bacterial species with asymmetric cell division, *Caulobacter crescentus* (Campos et al. 2014; Iyer-Biswas et al. 2014) and *Mycobacterium smegmatis* (Santi et al. 2013; Logsdon et al. 2017; Priestman et al. 2017), as well as the symmetrically dividing bacterium *Pseudomonas aeruginosa* (Deforet et al. 2015) have slightly positive values of α. In contrast, budding yeast *S. cerevisiae* (Di Talia et al. 2007; Soifer and Barkai 2014; Soifer et al. 2016; Chandler-Brown et al. 2017) and especially fission yeast *S. pombe* (Fantes 1977; Sveiczer et al. 1996) have negative values of α, implying a longer lingering of maternal effects.

Under the adder model of cell division, cells that are larger at birth divide at an earlier age because exponential growth in biomass generates the additive increment Δ more rapidly. From the form of the exponential-growth model (Equation 9.7), the division time for a cell of initial size V_0 under the adder model is

$$t_d = \frac{\ln[1 + (\Delta/V_0)]}{r}, \tag{9.8}$$

yielding a predicted decline in t_d with increasing V_0, consistent with observations in *E. coli* (Figure 9.4). As discussed below, in a dynamically growing population, this may lead to an equilibrium mean offspring size $> \Delta$, as offspring of large-size deviants will be promoted into the population at a higher rate than those of small-size deviants.

As a final caveat, it should be noted that even the expanded adder model seems to be not general enough (Delarue et al. 2017; Jun et al. 2018). As can be seen in Figure 9.4, the behavior of cells at both extreme ends of the size spectrum deviates from the model expectations. Even if the adder model is correct as a first-order approximation, the target value for change, Δ, appears to decline with increasing cell size, implying an additional contribution to compensatory growth not accounted for in the simplest model (Susman et al. 2018).

Division-size determination. The simple models just outlined provide a statistical view of the features of cell division, but leave unanswered questions regarding the molecular mechanisms by which cells determine that they have reached the critical threshold for division. Resolving this issue is a fundamental requirement for understanding how changes in cell sizes and division times might be accomplished by evolution.

One model invokes a burst of cell-division inhibitor produced at the time of cell division, which then gradually becomes diluted as cell volume increases. An alternative model invokes the gradual buildup of an activator molecule to the point at which a threshold concentration is exceeded. Simple mathematical constructs have been developed to explain the features of such systems (Sompayrac and Maaløe 1973; Amir 2014; Deforet et al. 2015; Soifer et al. 2016).

Where the underpinnings of cell-division time have been sought at the molecular level, inhibitor mechanisms have generally come to the fore. For example, the soil bacterium *Bacillus subtilis* determines the time of cell division by use of two-component interactive system (Weart et al. 2007; Chien et al. 2012). As a central hub, the tubulin-like cell-division protein (FtsZ) has a nearly constant concentration under all nutritional conditions. At high nutrient conditions, an inhibitor molecule (UgtP) oligomerizes with FtsZ preventing formation of the cytokinetic ring until a relatively large cell size (containing more free FtsZ molecules) is attained, whereas under low nutrient conditions, UgtP is sequestered away from FtsZ, allowing division at a smaller cell size. *E. coli* utilizes a different inhibitor mechanism to determine the time of division. In this case, an inhibitor molecule oscillates back and forth between the cell poles, such that a minimum concentration exists at the cell midpoint; once the concentration drops below a critical point by growth dilution, cell division ensues (Lutkenhaus 2008).

Inhibitor mechanisms for division-time determination extend to yeasts. Again, clear mechanistic differences exist among species, although the numerous molecular details are ignored here. The fission yeast *S. pombe* utilizes a spatial gradient to sense its size – an activator of mitosis is centrally located, whereas an inhibitor of the activator has a gradient initiating at the cell poles; as the cell grows, the inhibitor concentration declines to the point at which mitosis is activated (Moseley et al. 2009). In contrast, in the budding yeast *S. cerevisiae* a short burst of synthesis of a mitosis inhibitor is elicited shortly after cell division in a size-independent manner (Turner et al. 2012; Schmoller et al. 2015; Litsios et al. 2019). Smaller cells, with a higher inhibitor concentration at birth, must then add more volume to reduce the inhibitor to its critical concentration to allow mitosis to proceed. A second protein, maintained at a constant concentration throughout most of the cell life cycle, plays a central role here – it acts as an inhibitor of the mitotic inhibitor, but only becomes effective upon increasing in abundance late in the growth cycle and reducing the latter to a low enough level to allow division initiation.

What is most remarkable here is that although these four systems all rely on mechanisms of inhibition to determine cell-division time, the molecular details are essentially nonoverlapping. As in the case of the regulation of ribosome biogenesis, this implies that over evolutionary time the basic machinery dictating the key life-history features of cells – size and age of reproduction – has been rewired on multiple occasions. How such modifications are made without imperiling the fitness of individuals with intermediate states is unclear, and constitutes a major challenge for evolutionary cell biology.

Aside from this rather unsettling conundrum, the simple systems outlined above do provide a clear path to achieving an understanding of the molecular basis for evolutionary changes in cell size/division time via alterations in the concentrations and/or activities of the products of as few as two genes, e.g., an inhibitor molecule and its interacting partner. In principle, for example, larger cell size can be achieved by increasing the burst size of the mitotic inhibitor upon cell division or by reducing the steady-state concentration of the inhibitor of the inhibitor.

Environmental determinants of cell size. Whatever the mechanism of cell-size regulation, it is clear that the concentration of the critical agent(s) must vary with environmental conditions. Cell size typically increases with nutrient availability, which under the adder model implies an effective increase in Δ. For example, in *E. coli,* by far the most closely studied species, cell volume increases exponentially with cell-division rate (Taheri-Araghi et al. 2015), a response first documented in in *Salmonella typhimurium* (Schaechter et al. 1958) and observed to different extents in many other bacteria (Jun et al. 2018). In *S. typhimurium* and *E. coli,* there is a $\sim$ 5-fold increase in cell volume over the full range of growth rates (Volkmer and Heinemann 2011; Si et al. 2017), whereas the full response in the photosynthetic cyanobacterium *Synechocystis* is a 1.5-fold increase in cell volume (Zavřel et al. 2019).

A positive relationship between cell volume and growth rate has also been documented in unicellular eukaryotes, although the response is often closer to linear than exponential. For example, the ciliate *Tetrahymena* exhibits a two-fold increase in cell volume with nutrient availability (Zalkinder 1979), and the budding yeast *S. cerevisiae* (Tyson et al. 1979; Ferrezuelo et al. 2012) and the green alga *Chlorella pyrenoidosa* (Prokop and Ricica 1968) both have five-fold ranges.

Given this near-universality of the positive physiological response of cell volume to growth rate, it too has often been ordained as a "growth law." Although the underlying molecular mechanisms remain unclear, a phenomenological model that fits the data quite well in *E. coli* (Amir et al. 2017; Jun et al. 2018; Si et al. 2019) is potentially informative. Here, the idea is linked to the fact that when growing at rapid rates, bacteria can have multiple nested genomes. This pileup of partially replicated genomes occurs when the rate of genome replication lags the rate of production of the remaining cellular constituents, providing a possible indication of high-growth conditions. Because the replication of each circular genome initiates at a single origin of replication, there are two of these in a cell for each genome-replication initiation.

If one considers the unit of cell volume to be the total parent-cell volume per origin of replication, V_c, then assuming the latter is independent of the growth rate, which the data suggest in *E. coli* (Si et al. 2019), the total cell volume can be represented as the product of V_c and the numbers of origins of replication. Letting the time to produce a new chromosome origin be t_o and the cell-division time be t_d, the mean number of origins of replication in mature cells is $2^{t_o/t_d}$ (Jun et al. 2018), e.g., if division of the chromosome and the cell is synchronized, $t_o = t_d$, and there are two origins (one on each complete chromosome) at the time of cell division. Using Equation 9.3 to define t_d then leads to

$$V = V_c \cdot 2^{t_o/t_d} = V_c e^{rt_o}. \tag{9.9}$$

Although t_o is not entirely independent of the population growth rate r, when the product is taken into consideration, this model fairly accurately fits the response of *E. coli* cell volume to cell growth rate, with an exponential response of V to r predicted when t_o is invariant. Moreover, recalling Equation 9.8, an additional prediction can be made under this model – the negative scaling of cell-division time with variation in size of birth (within a particular condition) is expected to become increasingly strong in growth media associated with reduced r. Results from *E. coli* grown on different growth media are quite consistent with this prediction (Figure 9.4).

There are some caveats with respect to this model. First, any number of other underlying scaling determinants beyond the numbers of origins of replication (and highly correlated with them) might play a key role. Indeed, rather different models proposed by Serbanescu et al. (2020) and by Bertaux et al. (2020), with a focus on partitioning of resources between ribosomes and unspecified division proteins, fit the data just as well. Second, given that we have already seen that the molecular details of ribosome biogenesis and commitment to division vary among species, one should be wary of Jacob's (1998) proclamation that "All that is true for *E. coli,* is true for the elephant." The unit-cell model cannot apply to eukaryotes, which always undergo a single genome replication per cell division, although in principle, one might invoke some other target of counting that increases with cell volume.

What remains particularly unclear is the extent to which the size-growth rate relationship is driven by adaptive processes, i.e., whether increasing cell volume under high nutrient conditions somehow enhances the cell-division rate beyond that expected under constant cell size. The model based on unit-cell volume actually makes no assumption about the benefits of a size shift, simply postulating that the shift is a by-product of chromosome replication rates lagging rates of cell division (Amir 2017). Below, another argument is made as to how, under the adder model, cells phenotypically shifted to larger sizes might passively accumulate in cultures growing with higher rates of cell division.

What also remains to be reconciled is the relationship between the plastic size-growth relationship seen within particular genotypic isolates noted here and the phylogenetic patterns associated with maximum-growth rates noted in the preceding chapter (Figure 8.5). Among heterotrophic bacterial species, there is a positive association between maximum cell-division rate and cell size, which is in agreement with the developmental-plasticity pattern. Also consistent with this pattern is a long-term selection experiment for higher growth rate in *E. coli,* which yielded a parallel response in cell volume (Figure 9.5).

In contrast, among eukaryotic species, maximum cell-division rates decline with increasing cell size (Figure 8.5), contrary to the within-species response to a shift in nutrient availability (Figure 9.6A). Why there is there a conflict between responses at the evolutionary and physiological levels in eukaryotes but not in prokaryotes? One possibility is that, despite retaining the physiological downshift in size under low-nutrient conditions, the total growth capacity of eukaryotic cells with increasing size is compromised owing to the reduction in efficiency of natural selection imposed by the increased power of random genetic drift (Chapter 8). By extension, if this hypothesis is correct, small- to moderate-sized bacterial species should retain the flexibility to jointly evolve large cell size and high growth rates (Figure 9.5), whereas eukaryotic cells should be much more constrained, possibly even with a negative correlation.

Finally, we consider the effects of temperature, one of the most widely varying environmental parameters and a central determinant of cell physiology. Essentially all biochemical reaction rates, membrane fluidity, and diffusion coefficients increase with increasing temperature. Given the positive association of cell size and growth rate in environments with constant temperature, one might expect a parallel response to temperature, with higher temperatures, which induce faster growth (within physiological limits), resulting in larger cell volumes. Unfortunately, there is remarkably little information on this matter, although in their seminal work, Schaechter et al. (1958) found that *Salmonella* cells grown at low temperature are substantially larger than those growing at identical rates (with lower nutrients) at higher temperatures. Their results suggest that temperature induces a different cell-size response to growth rate than does nutrient availability – to maintain a specific growth rate at lower temperatures, individual cells seemingly have to be larger (Figure 9.6B).

How generalizable is this sort of observation? There is a long history of thought on the relationship between organism size and temperature, mostly focused on multicellular species. Here, the general idea is that organisms living in cooler environments have larger body sizes (within and among species), ostensibly because reduced surface:volume ratios reduce the potential for heat loss. In deference to the originator of the idea, the pattern has come to be known as Bergmann's (1847) rule. Although its generality has been questioned for multicellular organisms (Riemer et al. 2018), it does appear to hold for microbes, although likely for different reasons than proposed for homeothermic vertebrates. In every study where the matter has been closely investigated, average cell volume declines with increasing temperature, while the growth rate increases. Such observations have been drawn from ciliates, flagellates, amoeboid heterotrophs, and diverse photoautotrophs, with an overall average $\sim$ 25% increase in cell volume typically accompanying a 10°C decline in temperature (Atkinson et al. 2003; Fu and Gong 2017; Zohary et al. 2020). If nothing else, such observations demonstrate that the positive association between cell size and growth rate found in different nutritional environments is not generalizable to other environmental effects.

Again, whereas such a universal temperature response across the Tree of Life might suggest that a general adaptive hypothesis is required for such behavior, but no general explanation has yet emerged for such patterns. Indeed, given the existence of size-selective predation and potential size-dependent outcomes of competitive interactions and physical-environmental effects, mortality rates are likely to be size-dependent, so it is by no means clear that large cell-size is uniformly favorable in environments with low temperature (or high nutrient levels). Thus, it is worth considering whether the physiological response to temperature change, running in the opposite direction to that induced by nutritional differences, is a by-product of the molecular mechanisms that set times to division. Future work in this area should look to the numerous experiments that have shown that when the translational capacity of ribosomes is compromised by chemical manipulation in *E. coli,* the phenotypic scaling between cell size and growth rate runs in opposite directions to the nutrient-based pattern (Scott et al. 2010; Jun et al. 2018; Serbanescu et al. 2020). Perhaps the same underlying mechanism applies to cold temperatures.

Scaling of Intracellular Features

It is well known that various organs, tissues, and other body parts scale with body size as multicellular organisms grow (Thompson 1917), a phenomenon known as developmental allometry. Less clear is the extent to which internal cellular features (including transcript and protein numbers, organelle numbers and size, etc.) scale as cells grow from birth to maturity. A general positive relationship between cellular components and cell volume can be expected, as the organelles and molecular constituents of cells have functional roles whose total demands typically increase with the volume of cell, but the precise pattern of scaling is less clear.

On the one hand, intracellular features might scale isometrically throughout growth (thereby keeping the concentrations of all constituents of the intracellular environment relatively constant). This is consistent with exponential growth in cell volume noted above, which implies the maintenance of constant growth capacity per unit cell volume regardless of cell size. On the other hand, as cells grow and experience reductions in the surface area:volume ratio, the effective availability of nutrients per unit biomass may be reduced. If so, altered investments in machinery associated with nutrient uptake and intracellular transport may be required, much like the responses of ribosome investment seen when cells are grown under different nutrient conditions.

For the few eukaryotic cellular traits with a modicum of data, isometric scaling appears to be the norm. For example, in yeasts, mitochondrial volume constitutes $\sim 1\%$ of cell volume throughout life in *S. cerevisiae* (Rafelski et al. 2012), $\sim 10\%$ in *Candida albicans* (Tanaka et al. 1985), and $\sim 9\%$ in *Cryptococcus neoformans* (Mochizuki et al. 1998). Isometric scaling is also true in HeLa cells, with the fractional volume of mitochondria being $\sim 10\%$ (Posakony et al. 1977). Throughout growth in *Euglena gracilis,* the plastid constitutes $\sim 16\%$ and the mitochondrion $\sim 6\%$ of the total cell volume (Pelligrini 1980). Likewise, in the green alga *Chlorella fusca,* the volumetric contributions of plastids, mitochondria, and vacuoles remain nearly constant, at 40, 3, and 10% respectively (Atkinson et al. 1974). Total vacuole volume also scales nearly isometrically in *S. cerevisiae,* constituting $\sim 6\%$ of cell volume throughout the cell cycle (Chan and Marshall 2014; Chan et al. 2016).

Compelling evidence for cell-volumetric control of organelle size derives from observations on the eukaryotic nucleus. In both *S. cerevisiae* and *S. pombe,* nuclear volume comprises a nearly constant ~ 6 to 8% of cell volume throughout cell growth (Jorgensen et al. 2007; Goehring and Hyman 2012). Transplants of nuclei from small to large cells reveal that the nucleus expands to the size expected given the host-cell volume. Such responses are not affected by the amount DNA in the nucleus, as similar responses are observed when DNA content is increased as much as 16-fold (Neumann and Nurse 2007). Similar responses have been seen in vertebrate cell cultures (Levy and Heald 2012). Notably, across a wide range of prokaryotic species (without nuclear envelopes or histone-packaging of chromosomes), nucleoid size also grows nearly isometrically with cell volume within the growth cycle (Gray et al. 2019).

Although the molecular mechanisms underlying homeostasis of cytoplasmic compositions throughout the cell cycle remain unknown (Chan and Marshall 2010, 2012; Goehring and Hyman 2012; Brangwynne 2013), the general picture emerging is that eukaryotic cells typically operate as bioreactors, with relatively constant internal compositions, until rapid remodeling takes place at the time of division. It remains to be seen, however, whether individual cellular features grow independently through time at roughly the same rate, or are somehow mutually guided via feedback associated with cell volume. These two alternative models make somewhat different predictions with respect to scaling relationships (Foundations 9.3). Passive homeostasis might simply arise from global changes in transcription rates in response to growth rate, thereby leading indirectly to coordinated assembly of subcellular compartments without the need for elaborate system-specific regulatory mechanisms.

What remains unclear is how the ontogenetic patterns noted here relate to among-species scaling patterns observed at the phylogenetic level (Chapter 8). Returning to the questions relating to cell size and growth rate in the previous section, are the prevailing statistical relationships seen between pairs of characters during development recapitulated over evolutionary time with the divergence of phylogenetic lineages, or can evolution promote shifts in cellular composition in arbitrary directions? An organism's repertoire of developmental and phenotypic plasticities sets the range of phenotypic combinations that can be achieved and tested by natural selection prior to genetic change, so in principle genetic alterations that simply hardwire a plastic response into a constitutively expressed phenotype may provide a readily accessible route to multivariate evolution. This very old idea (Baldwin 1896; Waddington 1942) remains controversial, but essentially suggests that evolution will typically exploit the lines of least resistance by genetically assimilating pre-existing possibilities, not very different than the conventional view of descent with modification.

If that is the case for intracellular architecture, then the observations noted above suggest that isometric scaling of eukaryotic cell parts should prevail at the phylogenetic level. Although the topic is largely unexplored, the kinds of phylogenetic scalings outlined in Chapters 7 and 8 provide compelling material for future investigation. Indeed, with its strong molecular basis, evolutionary cell biology provides a compelling platform for understanding the mechanistic links (or lack thereof) between allometric scaling relationships at the ontogenetic, environmental (physiological), and phylogenetic levels.

Phenotypic Variation in Cell Size and Division Time

Although the preceding discussion has focused largely on the average behavior of cell-growth features, the variation in cell traits generated by the stochasticity of events inherent in growth-related processes is nontrivial. Sources of variation for cell size and growth rate include: 1) variation in birth size owing to imperfect partitioning at cell division; 2) variation in numbers of ribosomes and of other critical molecules per cell, partly associated with variation in initial partitioning, but also from subsequent events such as transcription and translation; 3) inaccuracies in the growth-increment target; and 4) extrinsic variation in the microenvironment.

Numerous attempts have been made to model the steady-state distributions of cell size and division time incorporating one or more of these factors (e.g., Powell

1956; Scherbaum and Rasch 1957; Koch and Schaechter 1962; Tyson and Hannsgen 1985a,b; Taheri-Araghi et al. 2015; Jun et al. 2018). There is by no means uniformity in opinion on the forms of cell-feature distributions, and the statistical details will not be pursued here. However, it is worth noting that predicted patterns are often closely related to formal distributions derived in the early days of statistics for entirely different reasons. For example, the Yule (1925) distribution can be used to describe the situation in which a number of cell parts have to be duplicated during the cell-growth process, with each duplication occurring independently with fixed probability per unit time, and cell division occurring at the time of duplication of the final part. In contrast to this parallel (autonomous) view of cell growth, a Pearson Type III distribution describes a situation in which cell division takes place only after the completion of a series of consecutive (interdependent) steps, with each initiated step completed with a certain probability per unit time following the exit from the preceding step (Kendall 1948). Although these models do not strictly incorporate variability in size at birth, they do have features that are conceptually connected to the assumptions under the adder model, where a certain amount of cellular biomass must accrue before the cell divides. They also generate skewed distributions, with long tails to the right, and superficially similar to what is typically seen with real data (Figure 9.7).

A review of results from single-cell monitoring demonstrates that the magnitude of standing variation among genetically uniform cells is generally quite large. Observations from well-mixed laboratory cultures of unicellular species suggest that coefficients of variation (CV, equal to standard deviation divided by the mean) in the range of 0.1 to 0.5 are common for size at birth and maturity, incremental addition, and age at division (Table 9.1). Such CVs are substantially higher than those observed for morphometric traits in genetically variable samples of multicellular organisms, which are usually on the order of 0.05 to 0.10 (Lynch and Walsh 1998).

Owing to bursty transcription and translation (Chapter 21; Rhee et al. 2014; Cao and Grima 2020), high levels of cell-to-cell variation extend to the molecular level, and this likely feeds back to generate variation in cell life-history traits. For a diversity of prokaryotes and eukaryotes, the CV for the number of molecules of particular proteins $\simeq \overline{x}^{-0.2}$, where $\overline{x}$ is the mean number of proteins/cell (Vallania et al. 2014). The average number of protein molecules per genetic locus per cell ranges from 10 to 10^5 from the smallest to the largest cell types (Figure 7.4), implying CV $\simeq=$ 0.6 to 0.1, with some evidence suggesting that 0.1 may be close to the asymptotic lower limit for highly expressed proteins (Keren et al. 2015). The CV for protein numbers also increases with decreasing cell-division rates by a factor of ~ 3 over the whole range of growth rates (Keren et al. 2015).

Table 9.1. Coefficients of variation (CV, standard deviation divided by the mean) for growth-related features of cells.

Species	Trait	CV	Reference
Bacteria:			
Aerobacter cloacae	Generation time	0.18	Powell 1958

Azotobacter agilis	Elongation rate	0.10	Harvey et al. 1967
	Generation time	0.22	Harvey et al. 1967
Bacillus mycoides	Generation time	0.48	Powell 1956
Bacillus subtilis	Generation time	0.54	Powell 1956
Bacterium aerogenes	Generation time	0.30	Powell 1956
Escherichia coli	Elongation rate	0.08	Taheri-Araghi et al. 2015
	Division length	0.14	Taheri-Araghi et al. 2015
		0.120	Harvey et al. 1967
	Birth length	0.16	Taheri-Araghi et al. 2015
	Generation time	0.21	Taheri-Araghi et al. 2015
		0.28	Harvey et al. 1967
		0.30	Kiviet et al. 2014
	Added length	0.24	Taheri-Araghi et al. 2015
Proteus vulgaris	Generation time	0.32	Powell 1956
Pseudomonas aeruginosa	Generation time	0.14	Powell 1958
Serratia marcescens	Generation time	0.17	Powell 1958
	Generation time	0.14	Tyson 1989
Streptococcus faecalis	Generation time	0.27	Powell 1956
Eukaryotes:			
Saccharomyces cerevisiae	Length of G1 phase	0.46	Di Talia et al. 2007
Schizosaccharomyces pombe	Division length	0.07	Tyson 1989
Tetrahymena pyriformis	Generation time	0.12	Scherbaum and Rasch 1957
	Division size	0.12	Scherbaum and Rasch 1957

Stochastic partitioning of cell contents at division. As all of the studies in Table 9.1 involve single genotypes, the observed variance is due entirely to vagaries in the internal and external cellular environment. An unresolved issue in most studies of variation in multicellular organisms is the relative contribution of different sources to overall levels of variation (Lynch and Walsh 1998). However, for cellular traits a number of insights can be gained from first principles.

As will be seen in Chapter 21, stochastic birth and decay of transcripts and proteins can generate intrinsic noise with respect to molecular copy numbers. Here, we consider the ways in which the basic features of molecular segregation during cell division generates variation among progeny. Such stochastic inheritance can have an equally if not greater overall effect than intrinsic transcriptional noise for the simple reason that upstream variation in molecular abundance can further generate gene-expression noise, and vice versa. Such an outcome is a simple consequence of the structure of biology – a large fraction of cellular products are responsible in one or more ways for their own production (Kiviet et al. 2014).

For the simplest case of a cell containing n molecules at the time of division, with each being independently and randomly distributed to the two daughter cells with probability 1/2, the average number of molecules inherited per offspring cell is $\overline{n}_o = n/2$, but from the binomial sampling formula the variance (i.e., the square of the standard deviation) will be $\sigma^2_{n_0} = n(1/2)(1/2) = n/4$. The coefficient of variation is then $\mathrm{CV}(n_o) = \sigma_{n_o}/\overline{n}_o = 1/\sqrt{n}$, showing that relative to the mean, the standard deviation is inversely related to the square root of the number of molecules being partitioned. This simple principle predicts elevated CVs in small cells containing smaller numbers of molecules. It may also, in part, explain the reduction in CVs in traits in multicellular species, which might average out the noise from their constituent cells.

Additional sources of randomness during cell division can inflate the level of variation. The argument outlined in the previous paragraph assumes a situation in which each daughter cell draws from an identical cytoplasmic pool. If, however, the cell volume of daughter cells is unequal (owing to the imperfect positioning of the division septum), the coefficient of variation for offspring cells becomes inflated to

$$\mathrm{CV}(n_o) = \left(\frac{1 - [\mathrm{CV}(V)]^2}{\overline{n}} + \left[[\mathrm{CV}(V)]^2 \cdot \{ [\mathrm{CV}(n)]^2 + 1 \} \right] \right)^{0.5}, \tag{9.9}$$

where $\overline{n}$ is the average number of molecules per adult cell, and $\mathrm{CV}(V)$ and $\mathrm{CV}(n)$ are the coefficients of variation for offspring (sister-cell) volume and for the number of molecules per parental cell, respectively (Huh and Paulsson 2011). Several studies in bacteria suggest that $\mathrm{CV}(V)$ is on the order of 0.1 – 0.078 in *E. coli* (Trueba 1982), 0.072 in *Bacillus subtilis* (Nanninga et al. 1979), 0.121 in *Caulobacter crescentus* (Trueba 1982), and 0.060 in *Schizosaccharomyces pombe* (Johnson et al. 1979; Tyson 1989). $\mathrm{CV}(n)$ is typically of similar magnitude to that for $\mathrm{CV}(V)$ and relatively similar among species – 0.104 in *E. coli* (Schaechter et al. 1962; Harvey et al. 1967), 0.101 in *Azotobacter agilis* (Harvey et al. 1967), 0.109 in *Salmonella typhimurium* (Schaechter et al. 1962), 0.161 in the dinoflagellate *Gonyaulax polyedra* (Homma and Hastings 1989), and 0.067 in the yeast *S. pombe* (Tyson 1989).

Unless $\overline{n} < 100$, with $\mathrm{CV}(V)$ and $\mathrm{CV}(n)$ both < 0.1, it can be seen from Equation 9.9 that random partitioning of cell volume does not greatly elevate the level of variation in the inherited numbers of molecules beyond the binomial expectation, $1/\sqrt{\overline{n}}$. On the other hand, if $\mathrm{CV}(V) > 0.1$, the inflation can be greater than tenfold (Figure 9.8).

Eukaryotic cells have an additional layer of stochasticity in that molecules can be segregated into vesicles or organelles prior to cell division, which are then randomly partitioned among offspring cells. Huh and Paulsson (2011) provide a general expression for the variation rendered under this model, but if it assumed that the number of vesicles per cell are independently distributed, and that the molecules are randomly distributed among vesicles,

$$\mathrm{CV}'(n_o) \simeq \left(\frac{1}{\overline{n}} + \frac{\{1 + [\mathrm{CV}(n_o)]^2\}\{1 + [\mathrm{CV}(v)]^2\}}{\overline{v}} \right)^{0.5}, \tag{9.10}$$

where $\overline{v}$ and $\mathrm{CV}(v)$ are the mean and coefficient of variation of the number of vesicles per cell. From Equation 9.9, we know that $\mathrm{CV}(n_o) > 1/\sqrt{\overline{n}}$ and possibly as large as 10. Studies of mitochondrial inheritance in the fission yeast *S. pombe* (Jajoo et al. 2016) and of endosome inheritance in mammalian cell cultures (Bergeland et al. 2001) suggest that the partitioning of such organelles is only slightly less variable than the binomial expectation, which would imply $\mathrm{CV}(v) \simeq 1/\sqrt{v}$. In addition, we expect the mean number of vesicles ($\overline{v}$) to be much lower than the mean number of molecules ($\overline{n}$) per cell. Thus, it is clear that the stochastic partitioning of vesicles (described in the second fraction in Equation 9.10) can be a dominant source of intracellular variation unless there is some regulatory mechanism for controlling cargo partitioning among vesicles and vesicle partitioning among offspring cells. Moreover, variable organelle partitioning is likely to generate more phenotypic variation among cells than might be expected based just on organelle number. For example, because mitochondria are the sites of ATP production in eukaryotic cells, and ATP drives transcription and other cellular processes, mitochondrial partitioning during inheritance can have nonadditive effects on offspring cell performance (das Neves et al. 2010; Johnston et al. 2012).

Finally, it is worth noting that some cellular features can lead to a less variable pattern of inheritance of intracellular contents than expected by chance. For example, in *E. coli* (and many other bacteria) the genome is compacted into a centrally located nucleoid. The resultant mesh-like features serve as a barrier to the movement of ribosomes, which then become more concentrated towards cellular poles for purely physical reasons (Castellana et al. 2016). This may lead to a more even distribution of ribosome numbers in progeny cells than expected if each ribosome were drawn independently.

Phenotypic Variation and Adaptation

As explained in prior chapters, much of evolutionary change is not a product of natural selection, and as adaptive as they might seem superficially, certain kinds of changes can only be efficiently promoted by selection under a narrow subset of population-genetic conditions. Nonetheless, either unaware or unconvinced of such issues, numerous investigators have asserted that variation-inducing features, like those noted above, are not simple consequences of biophysical constraints, but have been advanced by natural selection as strategies for survival in variable environments. There is, however, a remarkable void of evidence for phenotypic variance serving an adaptive purpose, and good reasons to think otherwise.

The following provides an overview of the general consequences of phenotypic variation for the process of natural selection. First, we consider how nonheritable environmental noise, such as that induced by cellular stochasticity, reduces the response to directional selection on a trait by obscuring the genetic differences among members of a population. Second, we demonstrate how, even in the absence of genetic variation, selection can yield a transient (and in some cases persistent) change in the phenotypic properties of a cell lineage, provided the environmental deviations among individuals are at least partially heritable, as will often be the case for growth-related traits. Finally, we will return to the issue of whether phenotypic variation (within genotypes) is maintained by natural selection as a mechanism for coping with a variable environment.

Environmental variation and the efficiency of selection. One of the bedrock results of evolutionary theory concerns the nature of the underlying determinants of the resemblance between relatives. Understanding this issue is critical to understanding processes of adaptation. Although the process of natural selection will always proceed provided there is fitness-associated phenotypic variation upon which to operate, only the fraction of variation with a heritable genetic basis will lead to permanent evolutionary change. As will be shown in the following section, heritable environmental effects can also lead to some response to directional selection, but any such response is transient, quickly decaying away once the prevailing pattern of selection is terminated.

The central question here is the degree to which offspring phenotypes resemble those of their parents. For asexually reproducing cells, this is simply defined by the fraction of the phenotypic variation that is genetic in basis, a quantity known as the broad-sense heritability (or H^2) (Foundations 9.4). This key measure is readily estimated by taking a random sample of a population and regressing offspring on parental phenotypes (Lynch and Walsh 1998). The best-fit slope, which almost always falls in the range of 0.0 to 1.0, is equivalent to H^2 (Figure 9.9). Because total phenotypic variance is the sum of contributions from genetic and environmental effects, the higher the background noise from environmental causes, the lower the heritability of the trait.

Now imagine a parental population with phenotypic mean $\overline{P}_p$, with directional selection moving the parental mean to $\overline{P}'_p$, yielding a change of $S = \overline{P}'_p - \overline{P}_p$. This difference S in mean phenotypes prior to reproduction is generally referred to as the selection differential. As an example, Figure 9.9 shows a situation in which an initial phenotype distribution (black bell-shaped curve) is shifted to the right by viability selection (red curve). The diagonal line denotes the parent-offspring regression. If there were perfect transmission of phenotypes across generations, i.e., if $H^2 = 1$, the mean offspring phenotype would be identical to that of the selected parent generation, and the response to selection (R) would equal the selection differential. However, if there is environmental variance for the trait, such transmission will be less than perfect because the parental phenotypes deviate from their underlying genotypic values. If there is no genetic variation, there will be no permanent selection response at all. Summing up, for a population of asexually reproducing cells, the response to selection is simply

$$R = H^2 S \tag{9.11}$$

(Figure 9.8), showing that H^2 is equivalent to the fraction of the selection differential that is transmitted across generations. In a simple fashion, this result illustrates that the ability of natural selection to promote genetic change declines with increasing environmental variation.

Inheritance of environmental effects. Although a permanent response to directional selection requires the promotion of underlying genetic change, a transient response can sometimes be achieved in the absence of genetic variation. Because selection operates regardless of the source of phenotypic variation, if variation at the phenotypic level owing to intrinsic and/or extrinsic environmental effects is partly heritable across generations, the mean phenotype will still move in the direction of selection, even in the absence of genetic variation (Foundations 9.5). Unlike the situation with genetic change, however, such a shift will not be permanent. Rather, under persistent directional selection, the population mean phenotype is expected to reach an alternative stable state reflecting a balance between the directional force of selection operating on phenotypes and the erosion of progress each generation resulting from the dilution of inherited environmental effects. If selection is relaxed, all progress due to the inheritance of acquired environmental deviations will be quickly eroded away.

This sort of transient response to selection is expected to apply to any cellular feature that is partly inherited across generations. For example, any trait that is a function of the number of molecules within a cell (such as a metabolic rate) will naturally be subject to inheritance across cellular generations owing to the fact that the contents of progeny cells are derived immediately from parental-cell constituents, with the molecular composition subsequently undergoing turnover associated with continued production and degradation. Given that offspring in unicellular species inherit half of their parent-cell constituents, these kinds of effects are expected to be much more significant than in multicellular species.

These kinds of effects are of likely relevance to laboratory experiments that either intentionally or indirectly select for extreme phenotypes. For example, as noted above for the adder growth model, large adult cells yield large progeny cells (although not as large, on average, as themselves), which more rapidly reach the point of cell division. Smaller cells take a longer time to reach the requisite cell-volume increase Δ, and hence lag in terms of their contribution to the growing population. Although the descendants of deviant cells will gradually move back towards the expected offspring size of Δ, with imperfect cell division, extreme cell sizes will continuously be produced anew, recreating the biasing process. This verbal model needs to be worked out in a more formal manner, but it provides a potentially simple and general explanation for the consistent observation of cells becoming larger in environments with higher nutritional status that applies to both prokaryotes and eukaryotes.

A selection experiment by Yoshida et al. (2014) may be relevant here. Using a cell sorter, they selected for smaller cell size in cultures of *E. coli* for 22 consecutive days by allowing only the smallest 1% of reproducing cells to propagate to the next generation. Overall, a decline of $\sim 20\%$ mean size was observed, with the variance in cell size declining only slightly (implying that sufficient opportunity for selection, but not necessarily genetic variance, remained throughout the experiment). Sequencing the entire genome of one selected population revealed only a single nucleotide change, the relevance of which remained unclear.

Although the logic just outlined provides a simple argument for why one expects an elevated resemblance between parents and offspring associated with transiently heritable environmental effects, there has been some suggestion of an even higher correlation between colateral relatives within genetically uniform cultures of cells. For example, Sandler et al. (2015) found that the correlation between cell-division times in maternal and offspring lymphoblast cells is just 0.04, whereas that between sister cells is 0.71, and that between first-cousins is 0.58. They call this elevated correlation among cousins relative to that between mother and offspring cells the "cousin-mother inequality." Similar observations have been made with cell-lineage studies of several bacterial species (Powell 1958). For example, in *Aerobacter cloacae,* the correlation in cell-division time is -0.15 for mother-daughter cells, but 0.44 for sibs, and 0.19 for first cousins. Likewise, for *Serratia marcescens,* these correlations are, respectively, -0.20, 0.58, and 0.38. The reduced correlation between first cousins relative to that between sibs is consistent with a progressive dilution of shared effects, and Powell observed a still further decline for second cousins. Cultures of mammalian cancer and embryonic stem cells exhibit similar behavior (Froese 1964; Kuchen et al. 2020).

Superficially, these results suggest a mechanism of inheritance that is lost for one generation, and then regained in the next, with subsequent erosion of the correlation occurring among the parallel descendants of maternal lineages. This led to the claim that such reappearance of heritability cannot be explained by stochastic inheritance, and requires an underlying deterministic mechanism (Pearl Mizrahi et al. 2015; Sandler et al. 2015). Although a model can be set up in which an internal oscillator (putatively a circadian clock) operates with a periodicity such that first cousins are born at approximately the same time (Sandler et al. 2015), the following simple argument indicates that a deterministic mechanism is not at all necessary.

Imagine that parent cells have their division times determined by physiological effects experienced early in life, but that en route to division, additional resources are gained (or lost) that will influence the division times of their offspring, e.g., a burst of transcriptional/translational activity late in the maternal cell cycle. Upon fission, these resources will then be approximately equally allocated to the two progeny cells, causing a sib correlation in the population, but having little (if any) effect on the maternal-offspring correlation. Although sibs share maternal effects, only a fraction of these will be transmitted to the next generation (leading to a smaller first-cousin correlation, and a still smaller one for second cousins) (Staudte et al. 1996).

The adaptive value of phenotypic variation. We finally turn to the common argument that within-genotype phenotypic variation is molded by natural selection as a bet-hedging strategy to deal with environmental variation (Thattai and van Oudenaarden 2004; Kussell and Leibler 2005; Fraser and Kaern 2009; Eldar and Elowitz 2010; Zhuravel et al. 2010; Kiviet et al. 2014; Ackermann 2015; Jahn et al. 2015). Aside from the fact that cellular features exhibit quite substantial variation owing simply to the intrinsic stochasticities of cellular processes, there are several compelling theoretical reasons for thinking that such selection should be the exception rather than the norm. The focus here is not on major discrete phenotypic changes induced by environmental triggers (such as spore formation, or transition to motility), which in many cases almost certainly represent adaptive survival mechanisms, but rather on the continuous range of variation typically associated with quantitative traits such as growth rate, cell size, and metabolic rates.

First, one of the most substantive reasons for questioning assertions about adaptive phenotypic-variation relates to the fact that selection is agnostic with respect to the underlying genetic/environmental determinants of variation. If, for example, selection favors an extreme phenotype, when individuals at the extreme are largely there as a consequence of nongenetic effects, the ability of selection to promote individuals with a genetic predisposition to extreme trait values will be compromised. This is because individuals with particularly extreme genetic values will compete for promotion by natural selection with those with more average genetic values but higher variance in expression (Bull 1987). Thus, selection for variance-producing genotypes is difficult when levels if stochastic phenotypic variance are already high, and the likelihood of success is even lower if there is a genetic correlation between the expected genetic value of an individual and the conditional phenotype distribution around the expectation.

Second, selection on phenotypic variation is a second-order effect, as individual genotypes are not promoted on the basis of their own expected genotypic values but via the distribution of phenotypes of their descendants. Unless there is continuing fluctuating selection for individuals at the opposite phenotypic extremes at a sufficiently high rate, the link between genotypes and their ability to differentially generate variation will be weak. This will especially be the case for sexually reproducing species where recombination will progressively remove the disequilibrium between parental genotypic values and descendant phenotype distributions.

Although these arguments do not entirely rule out the possibility of direct selection for the production of broad phenotype distributions, they do indicate that any convincing support for such a form of adaptation should be accompanied by evidence that the preceding arguments can be dismissed. It is one thing to hypothesize on the optimality of a complex feature, but quite another to demonstrate that natural selection is actually capable of advancing such change.

As one example of further interpretative difficulties here, Hashimoto et al. (2016) used single-cell monitoring methods to demonstrate that the rate of exponential growth of a culture of *E. coli* with the same average cell-division time is elevated if there is variance around the mean, arguing that these results demonstrate a "fundamental benefit of noise for population growth." As we know that the rate of population expansion (r) is inversely related to cell doubling time (t_D) (Equation 9.2), this result was readily predictable in advance – for any absolute change in t_D, the increment in r with decreased t_D is greater than the decrease incurred with increased t_D. This behavior results simply because in a growing population, r is bounded above 0.0 and increases at an accelerating rate as t_D becomes small.

Consider, however, the situation in which the population is declining rather than increasing. In this case, a sublineage of cells with a certain absolute deviation in survival time below the average will experience a greater change in the rate of decline than will a sublineage with a positive deviation of the same absolute amount. Here, variation in the underlying trait enhances the rate of decline of the sublineage. This is not a trivial example for the simple reason that, on average, populations ultimately must go through equal periods of growth and decline, else the population will either go extinct or fill the universe.

More generally, the relationship between the level of variation and the rate of growth of a cell lineage can be seen to be a simple consequence of the form of the fitness function (Figure 9.10). If the relationship between phenotype and fitness is concave upward, the average fitness of a variable population will be greater than that of a population having the same mean phenotype but no variance. In contrast, if the fitness-phenotype relationship is concave downward, the opposite occurs – in this case, the boost in fitness from the upwardly deviating phenotypes is smaller than the loss of fitness in downwardly deviating phenotypes. An extreme case can be seen for the situation in which the trait is under stabilizing selection with the mean phenotype coinciding with the optimum – any deviation from the optimum will result in a decline in fitness. Only for the special situation in which the fitness function is perfectly linear is the influence of variation on fitness effectively neutral, owing to the fact that equal upward and downward phenotypic deviations have equivalent effects on fitness.

Finally, even these arguments are not ironclad, as they consider only the situation in which the phenotype distribution is symmetrically distributed about the mean. With asymmetric phenotype distributions, many alternative outcomes are possible, as the bulk of the phenotype distribution may reside in regions where the fitness function is either increasing or declining. The salient issue is that there is no general advantage to phenotypic variation. Although transient situations may arise in which variation is useful, the same may be said for periods in which it is detrimental.

The general conclusion then is that intrinsic variation in cellular processes results in unavoidable high levels of phenotypic variation among individuals, much higher than observed in multicellular species that undergo strong bottlenecks between soma and germline. As seductive as it is to attach an adaptive meaning to all things biological, the idea that intrinsic phenotypic variance is generally promoted by selective processes appears to be a substantial overstatement if not positively misleading.

Summary

- A broad swath of observations from a diversity of organisms have led to a number of patterns involving cellular responses to growth environments that are general enough to be labeled "growth laws" by microbial physiologists. One of these is a universal increase in the relative investment in ribosomes with increasing cell-division rate, presumably reflecting the conflict of the high energetic cost of ribosomes and their necessity for building cellular material.

- The response of cell-division rate to the concentration of a limiting nutrient follows a hyperbolic relationship similar to the Michaelis-Menten form for enzyme kinetics.

- The growth of cell volume within a cellular life cycle is typically exponential in form, consistent with reaction rates per cytoplasmic volume being nearly size-independent, and implying that larger cells accumulate biomass at a higher absolute rate.

- A wide array of prokaryotic and eukaryotic cells determine their division times by monitoring the total change in size, rather than by targeting a specific size or time, dividing only after a threshold amount of material has been added. Such behavior naturally leads to cell-size homeostasis, although the model is best viewed as a first-order approximation.

- The molecular mechanisms underlying the determination of growth-size thresholds often involve the products of just two or three genes, implying relatively simple evolutionary paths for altering cell size and division time.

- In all species that have been studied closely, cell size increases with the nutrient status of the environment, but decreases with increasing temperature. It remains unclear whether such shifts are adaptive in any way, and they may simply be inevitable by-products of the underlying molecular mechanisms by which cells commit to division.

- The directions of scaling of cell size and growth rate are concordant at the phylogenetic and physiological levels in prokaryotes, but discordant in eukaryotes. This may be a consequence of the reduction in the efficiency of natural selection for maximum growth rate, owing to random genetic drift, in eukaryotes of increasing size.

- The ontogenetic response of cell composition to cell volume during individual growth presents a third axis of bivariate scaling to consider. Most of the data suggest isometric ontogenetic scaling, such that the relative proportions of cell contents remain constant during cell growth.

- Numerous sources of stochastic variation, ranging from sporadic transcription / translation to random partitioning of cellular contents at division, result in considerable phenotypic variation among genetically identical cells, even in well mixed environments. The magnitude of such variation, which obscures the visibility of genetic differences to natural selection, is substantially greater in unicellular than in multicellular organisms.

- Although there has been considerable speculation that such high levels of phenotypic variation represent adaptations molded by natural selection to cope with variable environments, there is little empirical or theoretical support for this contention.

- Owing to the fact that binary fission results in substantial sharing of the contents of parent, offspring, and sib cells, unicellular lineages are subject to significant inheritance of nongenetic effects, which can lead to transient shifts in phenotypic values in the absence of genetic change.

Foundations 9.1. The scaling of ribosome number and cell growth rate. Although cells in nature commonly experience fluctuations in resource availability on time scales shorter than the cell-division time, it is instructive to consider the steady-state situation in a constant environment, as when cells are grown in a continuous-flow chemostat (Chapter 8). Under such conditions, the production rate of every biomolecule (per existing molecule) in the cell must be identical to the rate of overall cell growth, ensuring a steady-state cellular composition.

The rate of translation per cell, and hence the cellular growth rate, ultimately depends on the number of ribosomes and the number of mRNA transcripts that they encounter. Although translation also involves the use of accessory proteins (e.g., aminoacyl tRNA synthetases, elongation factor, and many others; Barenholz et al. 2016) and transfer RNAs, under steady-state growth, the abundance of such factors will be in constant proportion to that of the ribosomes, leaving the latter as a quantifiable indicator of the rate of translation, and hence cell growth. This argument assumes that cells are conservative with respect to the production of energetically expensive ribosomes, i.e., produce no more than needed to service the current mRNA pool. Here, we follow a derivation presented by Scott et al. (2010) to quantify this connection.

Letting M denote the total protein mass associated with a cell, and M_R denote the total protein mass associated with ribosomes and their affiliated proteins, i.e., "extended ribosomes," then $f_R = M_R/M$ is the fractional allocation of proteins to translation. Letting m_R denote the protein mass of a single extended ribosome, which will hereafter be simply abbreviated to ribosome, the number of ribosomes per cell is $N_R = M_R/m_R = f_R M/m_R$.

Assuming that all ribosomes are engaged in translation, and letting k_T denote the rate of translation (i.e., the rate at which amino acids are added to elongating protein chains, here assumed to be constant), and letting m_{AA} be the average mass of an amino acid, the rate of increase in cellular protein mass is

$$\frac{dM}{dt} = m_{AA} \cdot k_T \cdot N_R = \left(\frac{m_{\mathrm{AA}} \cdot k_T \cdot f_R}{m_R} \right) \cdot M. \tag{9.1.1a}$$

Because the mass of all components of the cell must increase at the same rate under steady-state conditions, and cell division must proceed at the same rate as growth in size, Equation 9.1.1a can also be written as

$$\frac{dM}{dt} = rM, \tag{9.1.1b}$$

with r denoting the per-capita rate of cell division. The solution of this expression is

$$M(t) = M(0) \cdot e^{rt}, \tag{9.1.1c}$$

where

$$r = m_{AA} \cdot k_T \cdot f_R/m_R, \tag{9.1.2a}$$

which can be condensed to a simpler form

$$r = K_R \cdot f_R, \tag{9.1.2b}$$

with $K_R = m_{AA}k_T/m_R$ being a measure of the translational capacity of the system (the rate of protein mass produced per unit mass of extended ribosomes).

Although the preceding derivation assumes that all ribosomes are actively engaged in translation, if a subfraction $f_{R,0}$ is inactive (independent of growth conditions), then

$$r = K_R \cdot (f_R - f_{R,0}), \tag{9.1.2c}$$

which rearranges to

$$f_R = f_{R,0} + \left(\frac{r}{K_R}\right). \tag{9.1.3}$$

The central assumptions in the preceding derivations are that the translation rate of engaged ribosomes (k_T) and the fraction of unoccupied ribosomes ($f_{R,0}$) are invariant with respect to growth rate. Under such conditions and subject to the constraint that $f_R \leq 1$, Equation 9.1.3 predicts a linear relationship between the fraction of protein invested in extended ribosomes and the rate of cell division, with the intercept being equivalent to the fraction of total cellular protein associated with unengaged ribosomes, and the slope ($1/K_R$) measuring the inverse of the translational capacity. If $f_{R,0}$ and K_R are functions of r, the scaling relationship in Equation 9.1.3 would be altered.

Foundations 9.2. Nutrient limitation and cell growth. In Foundations 9.1, an expression for the rate of cellular growth was derived in terms of ribosome processing. However, an alternative expression for the growth rate can be couched in terms of the rate of conversion of a limiting nutrient into biomass, again represented by the total mass of protein M. Under steady-state conditions, both approaches must yield equivalent answers for the rate of cell growth, as the rate of amino-acid uptake/biosynthesis must equal the rate at which amino acids are incorporated into proteins.

We first introduce the second approach, and then unify the two into a joint expression. Again following Scott et al. (2010), we let

$$\frac{dM}{dt} = c \cdot k_E \cdot M_E, \tag{9.2.1a}$$

where M_E is the summed mass of the enzymatic proteins involved in nutrient acquisition and conversion into amino acids,

$$k_E = k_{E,\max}\left(\frac{S}{K_S + S}\right), \tag{9.2.1b}$$

is the rate of nutrient acquisition per mass of enzyme protein, following the Michaelis-Menten form, which depends on the nutrient concentration (S), and the half-saturation constant (K_S), and c is a constant representing the conversion of the nutrient into M.

We now assume that the total protein in a cell (M) can be partitioned into three sectors (Figure 9.11): a fraction taken to be quantitatively (although not necessarily qualitatively) invariant with respect to cell physiology; a fraction consisting entirely of ribosomal proteins and other proteins associated with translation (extended ribosomes, as in Foundations 9.1); and a fraction associated with metabolic features that respond to nutritional changes. Letting these three fractions be f_Q, f_R, and f_P respectively, the system is constrained to obey

$$1 = f_Q + f_R + f_P. \tag{9.2.2}$$

Because f_Q is taken to be a constant, this means that increased investment in nutrient acquisition (f_P) necessitates a parallel reduction in investment in protein production (f_R).

Further letting f_E denote the fraction of protein mass in sector P devoted to uptake of the limiting nutrient, i.e., $f_E = M_E/M_P$, and recalling from Foundations 9.1 that $f_P = M_P/M$, Equation 9.2.1a expands to

$$\frac{dM}{dt} = (c \cdot k_E \cdot f_E \cdot f_P) \cdot M. \tag{9.2.3}$$

As in Foundations 9.1, the product within the parentheses is equivalent to the rate of exponential growth, which can be further abbreviated to

$$r = K_N \cdot f_P, \tag{9.2.4}$$

where $K_N = c \cdot k_E \cdot f_E$ can be viewed as the nutritional capacity of the system.

We next wish to generate a more general growth-rate expression taking into joint consideration the underlying details about both translation (Foundations 9.1) and nutrient uptake. The key point is that under balanced growth, the rate of nutrient conversion into biomass must be equivalent to the rate of protein production by ribosomes. There is in addition the constraint that the flexible fraction of the proteome must be apportioned into the fractions associated with translation (f_R) and nutrient provisioning (f_P).

As noted above, given that $f_R + f_P = 1 - f_Q$, there is an intrinsic tradeoff between the two processes. The maximum possible fractional allocation to ribosomes (or to the remaining pool) is $f_{R,\max} = (1 - f_Q)$, or in other words,

$$f_R = f_{R,\max} - f_P. \tag{9.2.5}$$

Recalling Equation 9.1.2c and substituting for f_R from the preceding expression,

$$r = K_R \cdot (f_{R,\max} - f_{R,0} - f_P), \tag{9.2.6}$$

where, as in Foundations 9.1, K_R is a measure of translational capacity, and $f_{R,0}$ is the fraction of investment in inactive ribosomes. Further substitution for f_P from Equation 9.2.4 and some rearrangement leads to the overall solution

$$r = K_R \cdot (f_{R,\max} - f_{R,0}) \cdot \left(\frac{K_N}{K_R + K_N} \right), \tag{9.2.7}$$

This expression provides a mechanistic link between nutrient uptake and conversion to protein biomass by ribosomes, in effect describing the situation in which the allocation to R and P proteins, f_R and f_P, is mutually adjusted such that the rate of intake of critical nutrients is matched by the rate of conversion into protein, subject to the constraint that these must sum to $1 - f_Q$. The fraction in large parentheses on the right is a function of the translation and nutritional capacities of the system, with the cell growth rate $r \to 0$ as $K_N \to 0$, and r asymptotically approaching a maximum value as $K_N \to \infty$. Because the fraction on the right equals 0.5 when $K_R = K_N$, the ribosomal capacity can be viewed as the half-saturation constant for nutrient capacity. Thus, despite the added complexities, the overall expression for r retains the form of a Monod growth equation, with $r_{\max} = K_R \cdot (f_{R,\max} - f_{R,0})$.

This kind of partitioning model can be taken in a number of other interesting directions. For example, it has long been known that cells under chronically high nutrient levels often switch to seemingly inefficient modes of energy production, e.g., engagement in fermentation processes, which leave incompletely oxidized products such as acetate or lactate, as opposed to the citric acid cycle, which oxidizes glucose all the way down to CO_2. Such metabolic overflow, or energy spillage, at high resource levels can be explained by the fact that the machinery underlying fermentation processes involves many fewer enzymes than that required for the citric acid cycle (Molenaar et al. 2009; Basan et al. 2015). The hypothesis here is that when the external carbon supply is high, cells can increase the investment in the protein machinery necessary for biosynthesis by reducing the investment in the enzymes necessary for input into such pathways. In contrast, when the nutrient supply is low, investing more heavily in carbon metabolism allows cells to maximize the limited but potential flux that can be directed towards biosynthesis.

Bertaux et al. (2020) and Serbanescu et al. (2020) have extended the preceding model to incorporate additional sector partitioning, e.g., cell division. These extensions allow for analysis of the size-growth rate relationship discussed in the text. There is room for caution in overinterpreting the good fits of models like these, as a large number of parameters are employed, not all of which are based on extrinsic estimates. Their value is in helping to clarify the importance of broad classes of potential underlying mechanisms that can be followed up by further empirical study.

Foundations 9.3. Scaling models for the development of cellular features. In light of what little we know about the mechanisms driving the quantitative relationships between cells and their parts during cell growth, consideration of alternative models may be informative, particularly if they predict alternative patterns of scaling.

Here we evaluate two fairly general models, in both cases assuming exponential growth of the cell in terms of total volume following Equation 9.7. First, consider the situation in which a cellular feature grows exponentially and autonomously (i.e., independent of cell volume, V) at rate β, such that the expected phenotypic value at time t is

$$z_t = z_0 e^{\beta t}, \tag{9.3.1}$$

where z_0 is the phenotypic value at cell birth. Log transforming Equations 9.7 and 9.3.1, solving the first expression for t, and substituting into the latter, we obtain

$$\log(z_t) = \left(\frac{\beta}{r}\right) \log(V_t) + c, \tag{9.3.2a}$$

where

$$c = \log(z_0) - \left(\frac{\beta}{r}\right) \log(V_0), \tag{9.3.2b}$$

is the intercept of a log-log plot of z_t vs. V_t throughout developmental progression. Noting that c is a constant determined by the size of the trait and cell volume at birth (as well as the growth parameters β and r), this model predicts an allometric (power law; Chapter 8) relationship, with the slope providing an estimate of the ratio of growth rates (β/r). If the slope is equal to 1.0, then β must equal r, implying isometric growth.

Now consider the situation in which growth of the trait is directly linked to the growth in cell volume via some sort of regulatory mechanism (Harris and Theriot 2016), such that

$$\frac{dz}{dt} = \beta \cdot V_t = \beta \cdot V_0 e^{rt}, \tag{9.3.3}$$

the solution of which is

$$z_t = \left(\frac{\beta}{r}\right) V_t + c, \tag{9.3.4a}$$

with

$$c = z_0 - \left(\frac{\beta}{r}\right) V_0. \tag{9.3.4b}$$

Note that the key scaling parameter is again the ratio of growth rates, β/r. However, in contrast to the volume-independent model, where there is linear scaling between the log-transformed values of z_t and V_t, when trait growth is coupled directly to cell volume, the scaling is linear on the original scale of measurement. If $\beta \simeq r$, which the data in the text suggest for volumetric traits, these two models will be difficult to distinguish based on growth-trajectory data alone. In both cases, the relationship will be essentially linear on the original scale of measurement, although only the autonomous-growth model predicts a zero intercept on this scale.

Foundations 9.4. Parent-offspring resemblance and the response to selection. The phenotypic measure of a particular trait in a specific individual can be viewed as the sum of its expected value given its genotypic composition, G, and a deviation from that expectation, E, owing to both internal effects associated with stochastic molecular behavior and external effects associated with physical, chemical, and biological aspects of the environment,

$$P = G + E. \tag{9.4.1}$$

The genotypic value G can be thought of as the average phenotypic measure expected if a large number of individuals of the same genotype were monitored in an identical environmental setting. The environmental effect E summarizes the net positive or negative deviations around G, and has a mean (over all individuals) equal to zero and variance among individuals of σ_E^2 (Lynch and Walsh 1998). Provided there is no genotype-environment covariance (i.e., environmental deviations are independent of the genetic background), the total phenotypic variance in the population is the sum of the genetic and environmental variance components,

$$\sigma_P^2 = \sigma_G^2 + \sigma_E^2. \tag{9.4.2}$$

If the offspring of measured parents are allowed to develop to the same stage as the parents and then measured, one can produce a parent-offspring regression, which is equivalent to the straight line that best describes the overall relationship (Figure 9.9). The slope of a best fit line is known to be equal to the ratio of the covariance between x and y variables (denoted as $\sigma(x, y)$, with the two variables here being offspring and parent phenotypes) and the variance of the x variable (denoted as $\sigma^2(x)$ for parental phenotypes). (For those unfamiliar with statistics, a variance is the average squared deviation of measures from the mean, whereas a covariance is the average cross-product of x and y deviations from their respective means). Letting o and p denote offspring and parents, assuming asexual reproduction, the covariance between offspring and parent pairs expands to

$$\sigma(P_o, P_p) = \sigma[(G_o + E_o), (G_p + E_p)]. \tag{9.4.3a}$$

Assuming that the environmental deviations in different generations are uncorrelated (i.e., not inherited, an assumption relaxed in Foundations 9.5), there can only be covariance between the genetic values, so

$$\sigma(P_o, P_p) = \sigma(G_o, G_p), \tag{9.4.3b}$$

and because parents and offspring have identical genetic values in an asexual population, the genetic covariance is the same as the genetic variance,

$$\sigma(P_o, P_p) = \sigma_G^2. \tag{9.4.3c}$$

The expected slope of the parent-offspring regression is then the ratio of Equations 9.4.3c and 9.4.2,

$$H^2 = \frac{\sigma_G^2}{\sigma_G^2 + \sigma_E^2}. \tag{9.4.4}$$

This quantity, which is usually referred to as the broad-sense heritability, is simply the fraction of the total phenotypic variance attributable to genetic causes. Further aspects concerning the phenotypic covariances among clonal relatives can be found in Jun et al. (2018). Slight modifications are required under sexual reproduction, as parents only transmit half their genetic value to their progeny (Lynch and Walsh 1998).

Foundations 9.5. Transient response to selection without genetic change. Under the adder model for growth, Δ is equivalent to the expected increase in cell volume between cell divisions, and the expected size at birth is also Δ. This, however, is only strictly true in the absence of selection on cell size. Imagine a clonal population of cells with some variation in the realized value of Δ experienced by individual cells, owing to the vagaries in intracellular and external environments, and the fact that cells do not divide with absolutely perfect symmetry.

With variation around the mean Δ, the size of an adult cell at the time of division can be expressed as

$$V_a = V_0 + \Delta + e_\Delta, \tag{9.5.1a}$$

where V_0 is the size at birth, Δ is the expected growth in size, and e_Δ is the deviation of the actual growth increment from Δ owing to background variation, assumed to have a mean value of zero and some variance σ^2_Δ. In the absence of selection, the expected value of V_0 is Δ, and the previous expression can be written as

$$V_a = 2\Delta + e_\Delta, \tag{9.5.1b}$$

with the expected offspring cell size being $\overline{V}_0 = \overline{V}_a/2 = \Delta$ because the expected value of e_Δ is equal to zero.

If, however, there is directional selection on cell size, the mean value $\overline{e}_\Delta$ is no longer equal to zero, as the cells with more extreme deviations are differentially promoted. Instead, in the first generation of selection, the average offspring cell size becomes

$$\overline{V}_0(1) = \Delta + (\overline{e}_\Delta/2)$$

assuming that on average half of the mean environmental deviation in the previous generation is transmitted to each offspring cell. If this same level of selection is continued for another generation, the mean becomes

$$\overline{V}_0(2) = \Delta + (\overline{e}_\Delta/2) + (\overline{e}_\Delta/4)$$

as a new deviation is added while half of the prior deviation is partially removed by 50% dilution. Using the series expansion

$$\sum_{i=1}^{t} x^i = \frac{x(1-x^t)}{1-x}, \tag{9.5.2}$$

with $x = 0.5$, after t generations of constant selection, the mean offspring size is

$$\overline{V}_0(t) = \Delta + \overline{e}_\Delta[1 - (1/2)^t] \tag{9.5.3}$$

which asymptotically approaches $\Delta + \overline{e}_\Delta$ as t increases.

This shows that the average size of cells in a population can quickly shift to a new value, with a deviation from the nonselection value Δ equal to the selection differential

$\overline{e}_\Delta$. The central point is that owing to the partial transmission of offspring deviations to subsequent generations, the mean phenotypes in a population are expected to change if selection operates on a cellular trait, even if there is no genetic basis for the deviations. However, in this case, the selection response is transient in that if selection is relaxed, the initial deviation $\overline{e}_\Delta$ declines by 50% each generation, rapidly returning offspring cell volume to Δ. In contrast, any genetic contribution to the selection response would remain following selection.

Finally, supposing extreme cells can sequester their excess endowment to a degree that allows greater than 50% retention, then the use of Equation 9.5.2 shows that an even greater transient boost can be obtained by selection on environmental deviations, e.g., with $x = 0.75$, $\overline{V}_0(t)$ has an asymptotic value of $\Delta + 3\overline{e}_\Delta$.

Literature Cited

Ackermann, M. 2015. A functional perspective on phenotypic heterogeneity in microorganisms. Nat. Rev. Microbiol. 13: 497-508.

Alberghina, F. A., E. Sturani, and J. R. Gohlke. 1975. Levels and rates of synthesis of ribosomal ribonucleic acid, transfer ribonucleic acid, and protein in *Neurospora crassa* in different steady states of growth. J. Biol. Chem. 250: 4381-4388.

Amir, A. 2014. Cell size regulation in bacteria. Phys. Rev. Lett. 112: 208102.

Amir A. 2017. Is cell size a spandrel? Elife 6: e22186.

Atkinson, A. W., Jr., P. C. John, and B. E. Gunning. 1974. The growth and division of the single mitochondrion and other organelles during the cell cycle of *Chlorella,* studied by quantitative stereology and three dimensional reconstruction. Protoplasma 81: 77-109.

Atkinson, D., B. J. Ciotti, and D. J. Montagnes. 2003. Protists decrease in size linearly with temperature: ca. 2.5% degrees C(-1). Proc. Biol. Sci. 270: 2605-2611.

Baldwin, J. M. 1896. A new factor in evolution. Amer. Natur. 30: 441451.

Barenholz, U., L. Keren, E. Segal, and R. A. Milo. 2016. A minimalistic resource allocation model to explain ubiquitous increase in protein expression with growth rate. PLoS One 11: e0153344.

Basan, M., S. Hui, H. Okano, Z. Zhang, Y. Shen, J. R. Williamson, and T. Hwa. 2015. Overflow metabolism in *Escherichia coli* results from efficient proteome allocation. Nature 528: 99-104.

Bergeland, T., J. Widerberg, O. Bakke, amd T. W. Nordeng. 2001. Mitotic partitioning of endosomes and lysosomes. Curr. Biol. 11: 644-651.

Bergmann, K. G. L. C. 1847. Über die Verhältnisse der wärmeokönomie der Thiere zu ihrer Grösse. Göttinger Studien 3: 595-708.

Bertaux, F., J. von Kügelgen, S. Marguerat, and V. Shahrezaei. 2020. A bacterial size law revealed by a coarse-grained model of cell physiology. PLoS Comput. Biol. 16: e1008245.

Boehlke, K. W., and J. D. Friesen. 1975. Cellular content of ribonucleic acid and protein in *Saccharomyces cerevisiae* as a function of exponential growth rate: calculation of the apparent peptide chain elongation rate. J. Bacteriol. 121: 429-433.

Bonven, B., and K. Gullov. 1979. Peptide chain elongation rate and ribosomal activity in *Saccharomyces cerevisiae* as a function of the growth rate. Mol. Gen. Genet. 170: 225-230.

Brangwynne, C. P. 2013. Phase transitions and size scaling of membrane-less organelles. J. Cell Biol. 203: 875-881.

Brown, C. M., and A. H. Rose. 1969. Effects of temperature on composition and cell volume of *Candida utilis.* J. Bacteriol. 97: 261-270.

Bryan, A. K., A. Goranov, A. Amon, and S. R. Manalis. 2010. Measurement of mass, density, and volume during the cell cycle of yeast. Proc. Natl. Acad. Sci. USA 107: 999-1004.

Bull, J. J. 1987. Evolution of phenotypic variance. Evolution 41: 303-315.

Campos, M., I. V. Surovtsev, S. Kato, A. Paintdakhi, B. Beltran, S. E. Ebmeier, and C. Jacobs-Wagner. 2014. A constant size extension drives bacterial cell size homeostasis. Cell 159: 1433-1446.

Cao, Z., and R. Grima. 2020. Analytical distributions for detailed models of stochastic gene expression in eukaryotic cells. Proc. Natl. Acad. Sci. USA 117: 4682-4692.

Castellana, M., L. S. Hsin-Jung, and N. S. Wingreen. 2016. Spatial organization of bacterial transcription and translation. Proc. Natl. Acad. Sci. USA 113: 9286-9291.

Chan, Y.-H., and W. F. Marshall. 2010. Scaling properties of cell and organelle size. Organogenesis 6: 88-96.

Chan, Y.-H., and W. F. Marshall. 2012. How cells know the size of their organelles. Science 337: 1186-1189.

Chan, Y.-H., and W. F. Marshall. 2014. Organelle size scaling of the budding yeast vacuole is tuned by membrane trafficking rates. Biophys. J. 106: 1986-1996.

Chan, Y.-H., L. Reyes, S. M. Sohail, N. K. Tran, and W. F. Marshall. 2016. Organelle size scaling of the budding yeast vacuole by relative growth and inheritance. Curr. Biol. 26: 1221-1228.

Chandler-Brown, D., K. M. Schmoller, Y. Winetraub, and J. M. Skotheim. 2017. The adder phenomenon emerges from independent control of pre- and post-start phases of the budding yeast cell cycle. Curr. Biol. 27: 2774-2783.

Chien, A. C., S. K. Zareh, Y. M. Wang, and P. A. Levin. 2012. Changes in the oligomerization potential of the division inhibitor UgtP co-ordinate *Bacillus subtilis* cell size with nutrient availability. Mol. Microbiol. 86: 594-610.

das Neves, R. P., N. S. Jones, L. Andreu, R. Gupta, T. Enver, and F. J. Iborra. 2010. Connecting variability in global transcription rate to mitochondrial variability. PLoS Biol. 8: e1000560.

Deforet, M., D. van Ditmarsch, and J. B. Xavier. 2015. Cell-size homeostasis and the incremental rule in a bacterial pathogen. Biophys. J. 109: 521-528.

Delarue, M., D. Weissman, and O. Hallatschek. 2017. A simple molecular mechanism explains multiple patterns of cell-size regulation. PLoS One 12: e0182633.

Dennis, P. P., and H. Bremer. 1974. Macromolecular composition during steady-state growth of *Escherichia coli* B-r. J. Bacteriol. 119: 270-281.

Di Talia, S., J. M. Skotheim, J. M. Bean, E. D. Siggia, and F. R. Cross. 2007. The effects of molecular noise and size control on variability in the budding yeast cell cycle. Nature 448: 947-951.

Droop, M. R. 1973. Some thoughts on nutrient limitation in algae. J. Phycol. 9: 264-272.

Droop, M. R. 1974. The nutrient status of algal cells in continuous culture. J. Marine Biol. Assoc. United Kingdom 54: 825-855.

Droop, M. R. 1983. 25 years of algal growth kinetics: a personal view. Botanica Marina 26: 99-112.

Eldar, A., and M. B. Elowitz. 2010. Functional roles for noise in genetic circuits. Nature 467: 167-173.

Eun, Y. J., P. Y. Ho, M. Kim, S. LaRussa, L. Robert, L. D. Renner, A. Schmid, E. Garner, and A. Amir. 2018. Archaeal cells share common size control with bacteria despite noisier growth and division. Nat. Microbiol. 3: 148-154.

Fantes, P. A. 1977. Control of cell size and cycle time in *Schizosaccharomyces pombe*. J. Cell Sci. 24: 51-67.

Ferrezuelo, F., N. Colomina, A. Palmisano, E. Garí, C. Gallego, A. Csikász-Nagy, and M. Aldea. 2012. The critical size is set at a single-cell level by growth rate to attain homeostasis and adaptation. Nat. Commun. 3: 1012.

Forchhammer, J., and L. Lindahl. 1971. Growth rate of polypeptide chains as a function of the cell growth rate in a mutant of *Escherichia coli* J. Mol. Biol. 55: 563-568.

Fraenkel, D. G., and F. C. Neidhardt. 1961. Use of chloramphenicol to study control of RNA synthesis in bacteria. Biochim. Biophys. Acta 53: 96-110.

Fraser, D., and M. Kaern. 2009. A chance at survival: gene expression noise and phenotypic diversification strategies. Mol. Microbiol. 71: 1333-1340.

Freyssinet, G., and J. A. Schiff. 1974. The chloroplast and cytoplasmic ribosomes of *Euglena:* II. Characterization of ribosomal proteins. Plant Physiol. 53: 543-554.

Froese, G. 1964. The distribution and interdependence of generation times of HeLa cells. Exp. Cell Res. 35: 415-419.

Fu, R., and J. Gong. 2017. Single cell analysis linking ribosomal (r)DNA and rRNA copy numbers to cell size and growth rate provides insights into molecular protistan ecology. J. Eukaryot. Microbiol. 64: 885-896.

Godin, M., et al. 2010. Using buoyant mass to measure the growth of single cells. Nat. Methods 7: 387-390.

Goehring, N. W., and A. A. Hyman. 2012. Organelle growth control through limiting pools of cytoplasmic components. Curr. Biol. 22: R330-R339.

Gray, W. T., S. K. Govers, Y. Xiang, B. R. Parry, M. Campos, S. Kim, and C. Jacobs-Wagner. 2019. Nucleoid size scaling and intracellular organization of translation across bacteria. Cell 177: 1632-1648.

Harris, L. K., and J. A. Theriot. 2016. Relative rates of surface and volume synthesis set bacterial cell size. Cell 165: 1479-1492.

Harvey, R. J., A. G. Marr, and P. R. Painter. 1967. Kinetics of growth of individual cells of *Escherichia coli* and *Azotobacter agilis.* J. Bacteriol. 93: 605-617.

Hashimoto, M., T. Nozoe, H. Nakaoka, R. Okura, S. Akiyoshi, K. Kaneko, E. Kussell, and Y. Wakamoto. 2016. Noise-driven growth rate gain in clonal cellular populations. Proc. Natl. Acad. Sci. USA 113: 3251-3256.

Homma, K., and J. W. Hastings. 1989. Cell growth kinetics, division asymmetry and volume control at division in the marine dinoflagellate *Gonyaulax polyedra:* a model of circadian clock control of the cell cycle. J. Cell Sci. 92: 303-318.

Huh, D., and J. Paulsson. 2011. Random partitioning of molecules at cell division. Proc. Natl. Acad. Sci. USA 108: 15004-15009.

Iyer-Biswas, S., C. S. Wright, J. T. Henry, K. Lo, S. Burov, Y. Lin, G. E. Crooks, S. Crosson, A. R. Dinner, and N. F. Scherer. 2014. Scaling laws governing stochastic growth and division of single bacterial cells. Proc. Natl. Acad. Sci. USA 111: 15912-15917.

Jacob, F. 1998. The Statue Within: an Autobiography. Cold Spring Harbor Laboratory Press, Cold Spring Harbor, NY.

Jahn, M., S. Günther, and S. Müller. 2015. Non-random distribution of macromolecules as driving forces for phenotypic variation. Curr. Opin. Microbiol. 25: 49-55.

Jajoo, R., Y. Jung, D. Huh, M. P. Viana, S. M. Rafelski, M. Springer, and J. Paulsson. 2016. Accurate concentration control of mitochondria and nucleoids. Science 351: 169-172.

Johnson, B. F., G. B. Calleja, I. Boisclair, and B. Y. Yoo. 1979. Cell division in yeasts. III. The biased, asymmetric location of the septum in the fission yeast cell, *Schizosaccharomyces pombe.* Exp. Cell Res. 123: 253-259.

Johnston, I. G., B. Gaal, R. P. Neves, T. Enver, F. J. Iborra, and N. S. Jones. 2012. Mitochondrial variability as a source of extrinsic cellular noise. PLoS Comput. Biol. 8: e1002416.

Jorgensen, P., N. P. Edgington, B. L. Schneider, I. Rupes, M. Tyers, and B. Futcher. 2007. The size of the nucleus increases as yeast cells grow. Mol. Biol. Cell 18: 3523-3532.

Jun, S., F. Si, R. Pugatch, and M. Scott. 2018. Fundamental principles in bacterial physiology-history, recent progress, and the future with focus on cell size control: a review. Rep. Prog. Phys. 81: 056601.

Kendall, D. G. 1948. On the role of variable generation time in the development of a stochastic birth process. Biometrika 35: 316-330.

Keren, L., D. van Dijk, S. Weingarten-Gabbay, D. Davidi, G. Jona, A. Weinberger, R. Milo, and E. Segal. 2015. Noise in gene expression is coupled to growth rate. Genome Res. 25: 1893-1902.

Kimball, R. F., T. O. Casperson, G. Svensson, and L. Carlson. 1959. Quantitative cytochemical studies on *Paramecium aurelia.* I. Growth in total dry weight measured by the scanning interference microscope and x-ray absorption methods. Exp. Cell. Res. 17: 160-172.

Kiviet, D. J., P. Nghe, N. Walker, S. Boulineau, V. Sunderlikova, and S. J. Tans. 2014. Stochasticity of metabolism and growth at the single-cell level. Nature 514: 376-379.

Koch, A. L., and M. Schaechter. 1962. A model for statistics of the cell division process. J. Gen. Microbiol. 29: 435-454.

Krásný, L., and R. L. Gourse. 2004. An alternative strategy for bacterial ribosome synthesis: *Bacillus subtilis* rRNA transcription regulation. EMBO J. 23: 4473-4483.

Kuchen, E. E., N. B. Becker, N. Claudino, and T. Höfer. 2020. Hidden long-range memories of growth and cycle speed correlate cell cycles in lineage trees. Elife 9: e51002.

Kussell, E., and S. Leibler. 2005. Phenotypic diversity, population growth, and information in fluctuating environments. Science 309: 2075-2078.

Lenski, R. E., and M. Travisano. 1994. Dynamics of adaptation and diversification: a 10,000-generation experiment with bacterial populations. Proc. Natl. Acad. Sci. USA 91: 6808-6814.

Levy, D. L., and R. Heald. 2012. Mechanisms of intracellular scaling. Annu. Rev. Cell Dev. Biol. 28: 113-135.

Litsios, A., et al. 2019. Differential scaling between G1 protein production and cell size dynamics promotes commitment to the cell division cycle in budding yeast. Nat. Cell Biol. 21: 1382-1392.

Liu, K., A. N. Bittner, and J. D. Wang. 2015. Diversity in (p)ppGpp metabolism and effectors. Curr. Opin. Microbiol. 24: 72-79.

Logsdon, M. M., P. Y. Ho, K. Papavinasasundaram, K. Richardson, M. Cokol, C. M. Sassetti,

A. Amir, and B. B. Aldridge. 2017. A parallel adder coordinates mycobacterial cell-cycle progression and cell-size homeostasis in the context of asymmetric growth and organization. Curr. Biol. 27: 3367-3374.

Lutkenhaus, J. 2008. Min oscillation in bacteria. Adv. Exp. Med. Biol. 641: 49-61.

Lynch, M., and J. B. Walsh. 1998. Genetics and Analysis of Quantitative Traits. Sinauer Assocs., Inc., Sunderland, MA.

Maitra, A., and K. A. Dill. 2015. Bacterial growth laws reflect the evolutionary importance of energy efficiency. Proc. Natl. Acad. Sci. USA 112: 406-411.

Metzl-Raz, E., M. Kafri, G. Yaakov, I. Soifer, Y. Gurvich, and N. Barkai. 2017. Principles of cellular resource allocation revealed by condition-dependent proteome profiling. Elife 6: e28034.

Mir, M., Z. Wang, Z. Shen, M. Bednarz, R. Bashir, I. Golding, S. G. Prasanth, and G. Popescu. 2011. Optical measurement of cycle-dependent cell growth. Proc. Natl. Acad. Sci. USA 108: 13124-13129.

Mochizuki, T. 1998. Three-dimensional reconstruction of mitotic cells of *Cryptococcus neoformans* based on serial section electron microscopy. Nihon Ishinkin Gakkai Zasshi 39: 123-127.

Molenaar, D., R. van Berlo, D. de Ridder, and B. Teusink. 2009. Shifts in growth strategies reflect tradeoffs in cellular economics. Mol. Syst. Biol. 5: 323.

Monod, J. 1949. The growth of bacterial cultures. Ann. Rev. Microbiol. 3: 371-394.

Moseley, J. B., A. Mayeux, A. Paoletti, and P. Nurse. 2009. A spatial gradient coordinates cell size and mitotic entry in fission yeast. Nature 459: 857-860.

Nanninga, N., L. J. Koppes, and F. C. de Vries-Tijssen. 1979. The cell cycle of *Bacillus subtilis* as studied by electron microscopy. Arch. Microbiol. 123: 173-181.

Neumann, F. R., and P. Nurse. 2007. Nuclear size control in fission yeast. J. Cell Biol. 179: 593-600.

Osella, M., E. Nugent, and M. Cosentino Lagomarsino. 2014. Concerted control of *Escherichia coli* cell division. Proc. Natl. Acad. Sci. USA 111: 3431-3435.

Parenteau, J., L. Maignon, M. Berthoumieux, M. Catala, V. Gagnon, and S. Abou Elela. 2019. Introns are mediators of cell response to starvation. Nature 565: 612-617.

Pearl Mizrahi, S., O. Sandler, L. Lande-Diner, N. Q. Balaban, and I. Simon. 2016. Distinguishing between stochasticity and determinism: examples from cell cycle duration variability. Bioessays 38: 8-13.

Pellegrini, M. 1980. Three-dimensional reconstruction of organelles in *Euglena gracilis* Z. II. Qualitative and quantitative changes of chloroplasts and mitochondrial reticulum in synchronous cultures during bleaching. J. Cell Sci. 46: 313-340.

Plaut, B. S., and G. Turnock. 1975. Coordination of macromolecular synthesis in the slime mould *Physarum polycephalum.* Mol. Gen. Genet. 137: 211-225.

Posakony, J. W., J. M. England, and G. Attardi. 1977. Mitochondrial growth and division during the cell cycle in HeLa cells. J. Cell Biol. 74: 468-491.

Potrykus, K., H. Murphy, N. Philippe, and M. Cashel. 2011. ppGpp is the major source of growth rate control in *E. coli.* Environ. Microbiol. 13: 563-575.

Powell, E. O. 1956. Growth rate and generation time of bacteria, with special reference to continuous culture. J. Gen. Microbiol. 15: 492-511.

Powell, E. O. 1958. An outline of the pattern of bacterial generation times. J. Gen. Microbiol. 18: 382-417.

Poyton, R. O. 1973. Effect of growth rate on the macromolecular composition of *Prototheca zopfii,* a colorless alga which divides by multiple fission. J. Bacteriol. 113: 203-211.

Priestman, M., P. Thomas, B. D. Robertson, and V. Shahrezaei. 2017. Mycobacteria modify their cell size control under sub-optimal carbon sources. Front. Cell Dev. Biol. 5: 64.

Prokop, A., and J. Ricica. 1968. *Chlorella pyrenoidosa* 7-11-05 in batch and in homogeneous continuous culture under autotrophic conditions. I. Growth characteristics of the culture. Folia Microbiol (Praha) 13: 353-361.

Rafelski, S. M., M. P. Viana, Y. Zhang, Y.-H. Chan, K. S. Thorn, P. Yam, J. C. Fung, H. Li, F. Costa Lda, and W. F. Marshall. 2012. Mitochondrial network size scaling in budding yeast. Science 338: 822-824.

Rhee, A., R. Cheong, and A. Levchenko. 2014. Noise decomposition of intracellular biochemical signaling networks using nonequivalent reporters. Proc. Natl. Acad. Sci. USA 111: 17330-17335.

Riemer, K., R. P. Guralnick, and E. P. White. 2018. No general relationship between mass and temperature in endothermic species. Elife 7: e27166.

Rosset, R., R. Monier, and J. Julien. 1964. RNA composition of *Escherichia coli* as a function of growth rate. Biochem. Biophys. Res. Comm. 15: 329-333.

Sandler, O., S. P. Mizrahi, N. Weiss, O. Agam, I. Simon, and N. Q. Balaban. 2015. Lineage correlations of single cell division time as a probe of cell-cycle dynamics. Nature 519: 468-471.

Santi, I., N. Dhar, D. Bousbaine, Y. Wakamoto, and J. D. McKinney. 2013. Single-cell dynamics of the chromosome replication and cell division cycles in mycobacteria. Nat. Commun. 4: 2470.

Schaechter, M., O. Maaloe, and N. O. Kjeldgaard. 1958. Dependency on medium and temperature of cell size and chemical composition during balanced grown of *Salmonella typhimurium.* J. Gen. Microbiol. 19: 592-606.

Schaechter, M., J. P. Williamson, J. R. Hood, Jr., and A. L. Koch. 1962. Growth, cell and nuclear divisions in some bacteria. J. Gen. Microbiol. 29: 421-434.

Scherbaum, O., and G. Rasch. 1957. Cell size distribution and single cell growth in *Tetrahymena pyriformis* Gl1. Acta Pathol. Microbiol. 41: 161-182.

Schmoller, K. M., J. J. Turner, M. Kõivomägi, and J. M. Skotheim. 2015. Dilution of the cell cycle inhibitor Whi5 controls budding-yeast cell size. Nature 526: 268-272.

Scott, M., C. W. Gunderson, E. M. Mateescu, Z. Zhang, and T. Hwa. 2010. Interdependence of cell growth and gene expression: origins and consequences. Science 330: 1099-1102.

Serbanescu, D., N. Ojkic, and S. Banerjee. 2020. Nutrient-dependent trade-offs between ribosomes and division protein synthesis control bacterial cell size and growth. Cell Rep. 32: 108183.

Si, F., G. Le Treut, J. T. Sauls, S. Vadia, P. A. Levin, and S. Jun. 2019. Mechanistic origin of cell-size control and homeostasis in bacteria. Curr. Biol. 29: 1760-1770.

Si, F., et al. 2017. Invariance of initiation mass and predictability of cell size in *Escherichia coli.*

Curr. Biol. 27: 1278-1287.

Soifer, I., and N. Barkai. 2014. Systematic identification of cell size regulators in budding yeast. Mol. Syst. Biol. 10: 761.

Soifer, I., L. Robert, and A. Amir. 2016. Single-cell analysis of growth in budding yeast and bacteria reveals a common size regulation strategy. Curr. Biol. 26: 356-361.

Sompayrac, L., and O. Maaloe. 1973. Autorepressor model for control of DNA replication. Nat. New Biol. 241: 133-135.

Staudte, R. G., J. Zhang, R. M. Huggins, and R. Cowan. 1996. A reexamination of the cell-lineage data of E. O. Powell. Biometrics 52: 1214-1222.

Susman, L., M. Kohram, H. Vashistha, J. T. Nechleba, H. Salman, and N. Brenner. 2018. Individuality and slow dynamics in bacterial growth homeostasis. Proc. Natl. Acad. Sci. USA 115: E5679-E5687.

Sveiczer, A., B. Novak, and J. M. Mitchison. 1996. The size control of fission yeast revisited. J. Cell Sci. 109: 2947-2957.

Taheri-Araghi, S., S. Bradde, J. T. Sauls, N. S. Hill, P. A. Levin, J. Paulsson, M. Vergassola, and S. Jun. 2015. Cell-size control and homeostasis in bacteria. Curr. Biol. 25: 385-391.

Tanaka, K., T. Kanbe, and T. Kuroiwa. 1985. Three-dimensional behaviour of mitochondria during cell division and germ tube formation in the dimorphic yeast *Candida albicans.* J. Cell Sci. 73: 207-220.

Tanouchi, Y., A. Pai, H. Park, S. Huang, R. Stamatov, N. E. Buchler, and L. You. 2015. A noisy linear map underlies oscillations in cell size and gene expression in bacteria. Nature 523: 357-360.

Tempest, D. W., J. R. Hunter, and J. Sykes. 1965. Magnesium-limited growth of *Aerobacter aerogenes* in a chemostat. J. Gen. Microbiol. 39: 355-366.

Thattai, M., and A. van Oudenaarden. 2004. Stochastic gene expression in fluctuating environments. Genetics 167: 523-530.

Thompson, D. A. 1917. On Growth and Form. Cambridge Univ. Press, Cambridge, UK.

Trueba, F. J. 1982. On the precision and accuracy achieved by *Escherichia coli* cells at fission about their middle. Arch. Microbiol. 131: 55-59.

Turner, J. J., J. C. Ewald, and J. M. Skotheim. 2012. Cell size control in yeast. Curr. Biol. 22: R350-R359.

Tyson, J. J. 1989. Effects of asymmetric division on a stochastic model of the cell division cycle. Math. Biosci. 96: 165-184.

Tyson, J. J., and K. B. Hannsgen. 1985a. The distributions of cell size and generation time in a model of the cell cycle incorporating size control and random transitions. J. Theor. Biol. 113: 29-62.

Tyson, J. J., and K. B. Hannsgen. 1985b. Global asymptotic stability of the size distribution in probabilistic models of the cell cycle. J. Math. Biol. 22:61-68.

Tyson, C. B., P. G. Lord, and A. E. Wheals. 1979. Dependency of size of *Saccharomyces cerevisiae* cells on growth rate. J. Bacteriol. 138: 92-98.

Vallania, F. L., M. Sherman, Z. Goodwin, I. Mogno, B. A. Cohen, and R. D. Mitra. 2014. Origin and consequences of the relationship between protein mean and variance. PLoS One 9: e102202.

Vila-Sanjurjo, A. 2008. Modification of the ribosome and the translational machinery during reduced growth due to environmental stress. EcoSal Plus 3(1).

Volkmer, B., and M. Heinemann. 2011. Condition-dependent cell volume and concentration of *Escherichia coli* to facilitate data conversion for systems biology modeling. PLoS One 6: e23126.

Voorn, W. J., and L. J. Koppes. 1998. Skew or third moment of bacterial generation times. Arch. Microbiol. 169: 43-51.

Waddington, C. 1942. Canalization of development and the inheritance of acquired characters. Nature 150: 563-565.

Waldron, C., and F. Lacroute. 1975. Effect of growth rate on the amounts of ribosomal and transfer ribonucleic acids in yeast. J. Bacteriol. 122: 855-865.

Warner, J. R., J. Vilardell, and J. H. Sohn. 2001. Economics of ribosome biosynthesis. Cold Spring Harb. Symp. Quant. Biol. 66: 567-74.

Weart, R. B., A. H. Lee, A. C. Chien, D. P. Haeusser, N. S. Hill, and P. A. Levin. 2007. A metabolic sensor governing cell size in bacteria. Cell 130: 335-347.

Weiße, A. Y., D. A. Oyarzún, V. Danos, and P. S. Swain. 2015. Mechanistic links between cellular trade-offs, gene expression, and growth. Proc. Natl. Acad. Sci. USA 112: E1038-E1047.

Yoshida, M., S. Tsuru, N. Hirata, S. Seno, H. Matsuda, B. W. Ying, and T. Yomo. 2014. Directed evolution of cell size in *Escherichia coli.* BMC Evol. Biol. 14: 257.

Yoshida, H., and A. Wada. 2014. The 100S ribosome: ribosomal hibernation induced by stress. Wiley Interdiscip Rev. RNA 5: 723-732.

Young, R., and H. Bremer. 1976. Polypeptide-chain-elongation rate in *Escherichia coli* B/r as a function of growth rate. Biochem. J. 160: 185-194.

Yule, G. U. 1925. Mathematical theory of evolution, based on the conclusions of Dr. J. C. Willis, F.R.S. Phil. Trans. Royal Soc. London Series B 213: 21-87.

Zalkinder, V. 1979. Correlation between cell nutrition, cell size and division control. Part I. Biosystems 11: 295-307.

Zavřel, T., M. Faizi, C. Loureiro, G. Poschmann, K. Stühler, M. Sinetova, A. Zorina, R. Steuer, and J. Červený. 2019. Quantitative insights into the cyanobacterial cell economy. Elife 8: e42508.

Zhu, M., X. Dai, and Y. P. Wang. 2016. Real time determination of bacterial *in vivo* ribosome translation elongation speed based on LacZα complementation system. Nucleic Acids Res. 44: e155.

Zhuravel, D., D. Fraser, S. St-Pierre, L. Tepliakova, W. L. Pang, J. Hasty, and M. Kaern. 2010. Phenotypic impact of regulatory noise in cellular stress-response pathways. Syst. Synth. Biol. 4: 105-116.

Zohary, T., G. Flaim, and U. Sommer. 2020. Temperature and the size of freshwater phytoplankton. Hydrobiol. doi.org/10.1007/s10750-020-04246-6.

Figure 9.1. Response of various cellular features associated with mRNA translation to changes in cellular growth rate. References: *Candida utilis* – Brown and Rose (1969); *Euglena gracilis* – Freysinnet and Schiff (1974); *Neurospora crassa* – Alberghina et al. (1975); *Physarum polycephalum* – Plaut and Turnock (1975); *Prototheca zopfii* – Poyton (1973); *Saccharomyces cerevisiae* – Boehlke and Friesen (1975), Waldron and Lacroute (1975), Bonven and Gullov (1979), Metzl-Raz et al. 2017; *Escherichia coli* – Rosset et al. (1964), Forchhammer and Lindahl (1971), Dennis and Bremer (1974), Young and Bremer (1976), Scott et al. (2010), Zhu et al. 2016; *Aerobacter aerogenes* – Fraenkel and Neidhardt (1961); Tempest et al. (1965).

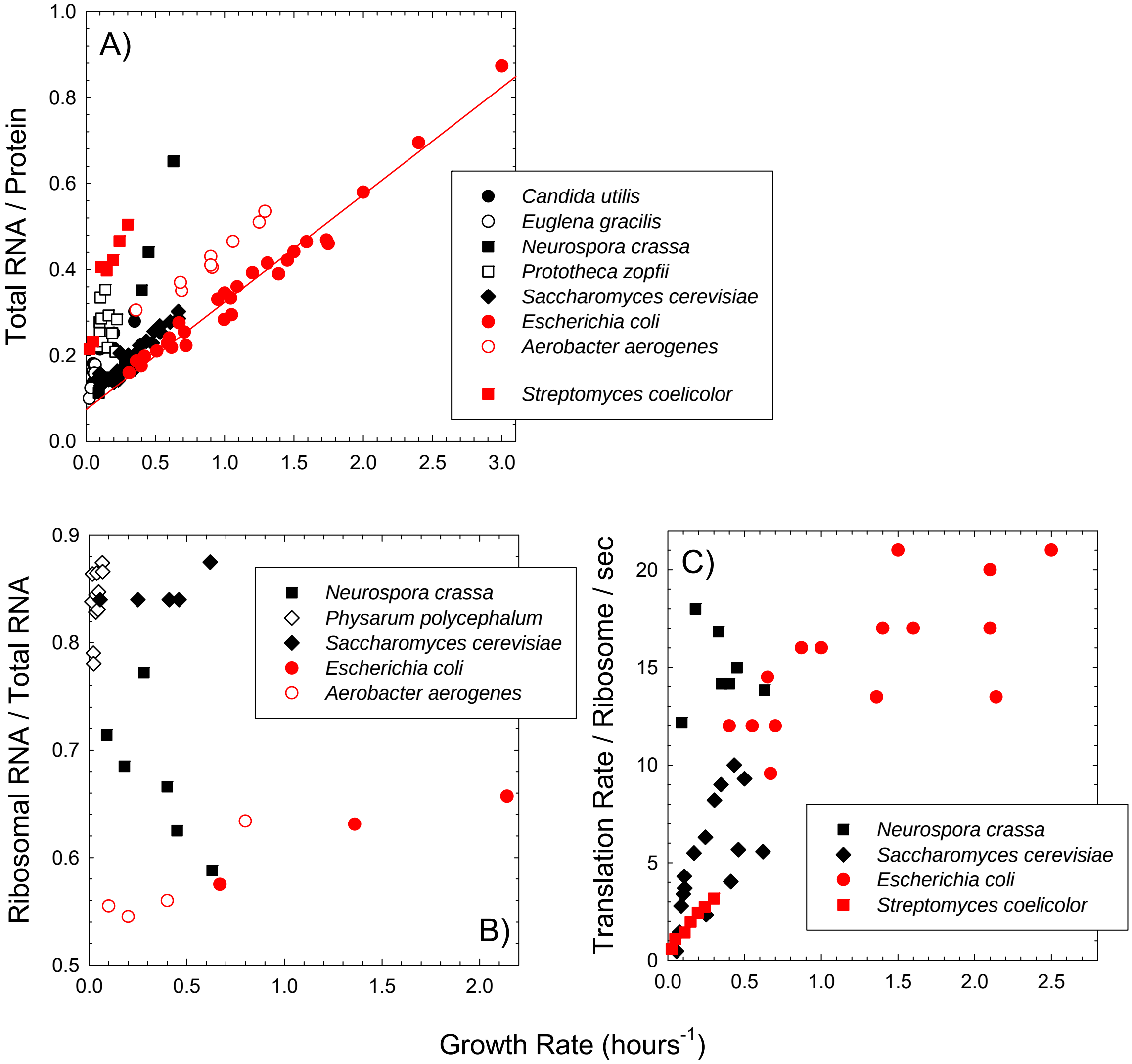

Figure 9.2. Various growth (r) and nutrient uptake (u) responses of the marine planktonic chrysophyte alga *Monochrysis lutheri* to various concentrations of vitamin B_{12}, recorded for populations of cells grown in a chemostat. The upper left and right graphs provide the relationships between the cell-division rate and external and internal nutrient concentrations. The lower-right graph illustrates the inverse linear relationship between r and $1/Q$, as predicted by Equation 9.5. For the lower left panel, the straight-line relationship for the rate of nutrient uptake is derived from Equation 9.4b, which rearranges to $(1/u) = (1/u_{\max}) + (K_u/u_{\max})(1/S)$. The data are from Droop (1973, 1974, 1984).

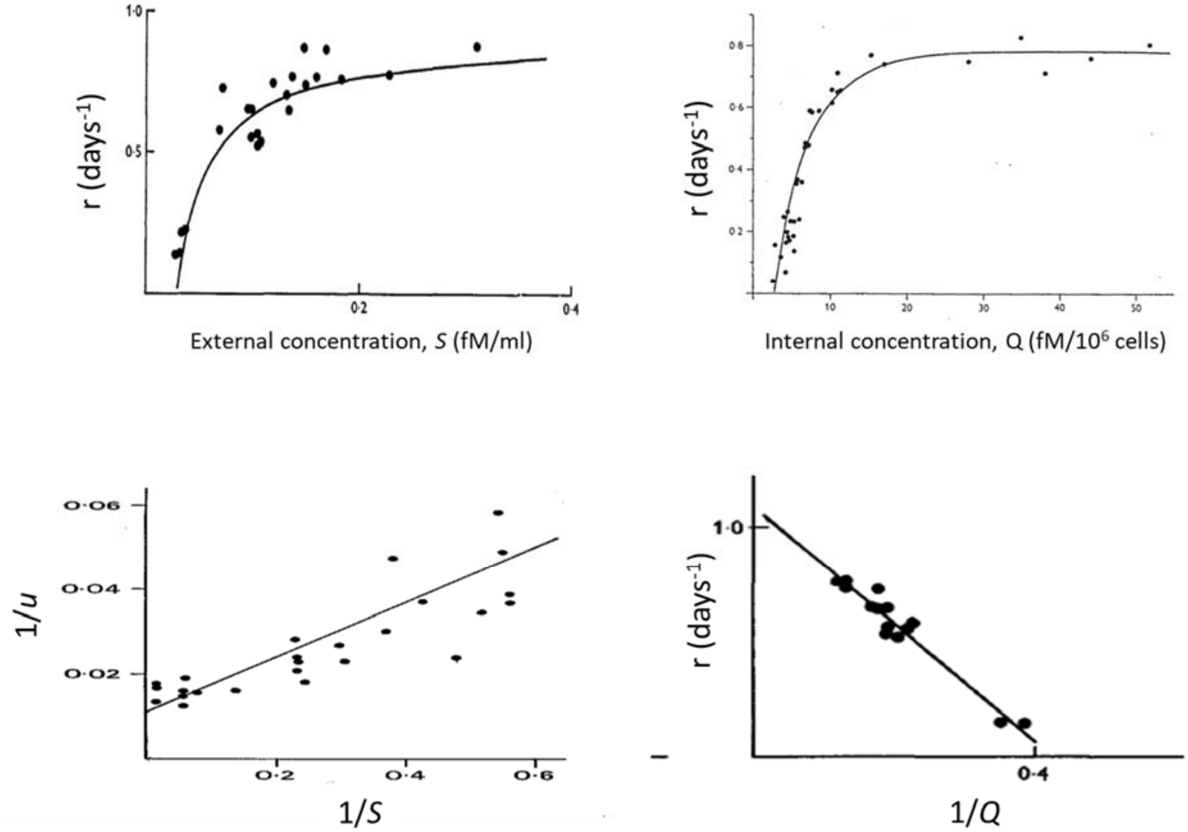

Figure 9.3. Expected relationship between cell volume at birth and at subsequent cell division under three alternative growth models. Δ serves as a reference point. Under the sizer model, regardless of the size at birth, the size at division always returns to 2Δ. Under the simplest form of the timer model, because of exponential growth, all cells grow by the same factor over a given duration, so individuals of extreme size produce offspring that are just as extreme; if there are stochastic deviations in offspring size or growth rates, the size distribution will diverge. Under the adder model, cells above or below the average still produce deviant progeny, but the average size of the progeny is less extreme than that of the parental cells, resulting in convergence of the cell-size distribution to an equilibrium.

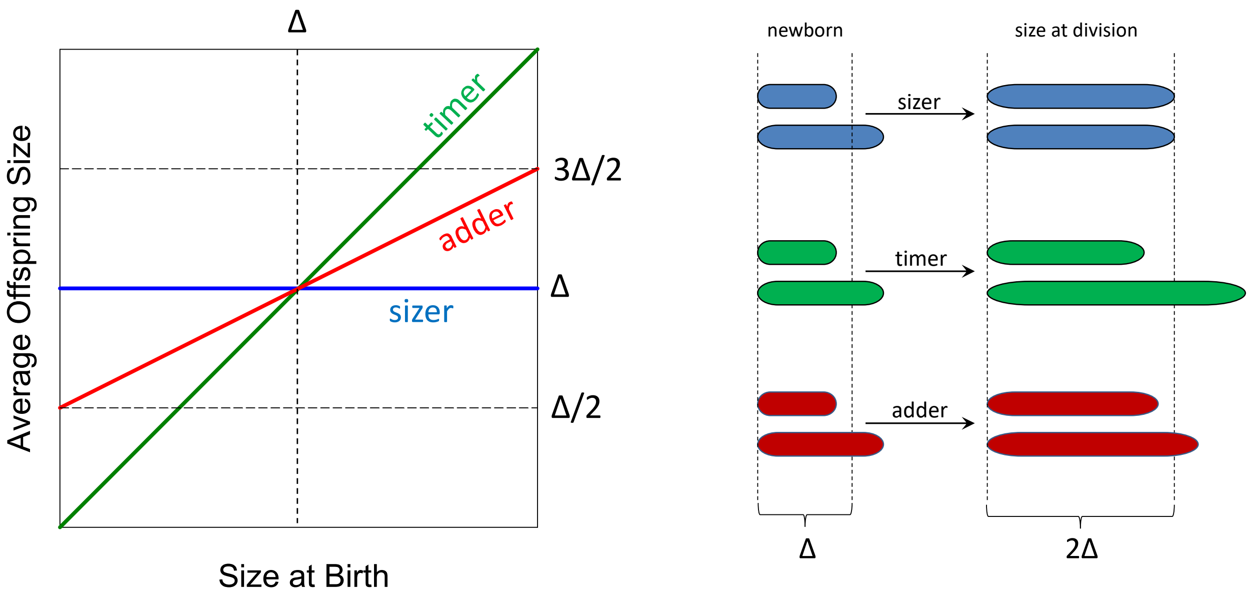

Figure 9.4. Evidence in favor of the adder model for *E. coli* grown in different media. Proceeding from left to right, the growth media are increasingly rich sources of energy, carbon, and other nutrients. **Upper panel)** By looking at individual cells within each medium (at a constant concentration), it can be seen that the growth increments to maturity (Δ) are nearly independent of the size at birth. **Lower panel)** The inverse relationship between the cell-division time and cell volume at birth becomes progressively stronger in media that support lower growth rates. In the upper and lower panels, respectively, size is presented as cell length and cell volume, although the two are directly proportional, given that *E. coli* cells are nearly cylindrical in shape. Note that the adder model only provides a first-order approximation, as cells at the extremes of the size range deviate from expectations. From Taheri-Araghi et al. (2015).

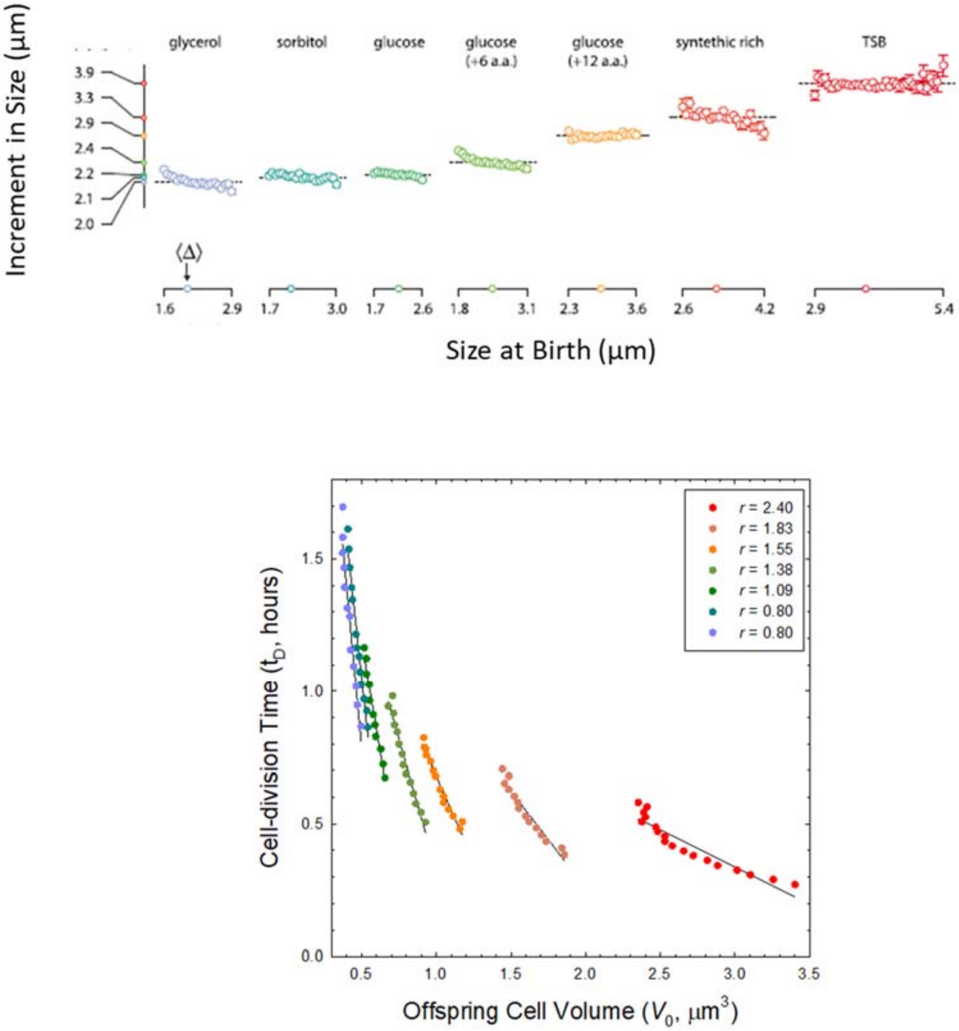

Figure 9.5. Evolutionary trajectories of cell-division rates and cell volume in a 10,000 generation experiment in which *E. coli* was subjected to persistent selection for higher growth rate. From Lenski and Travisano (1994).

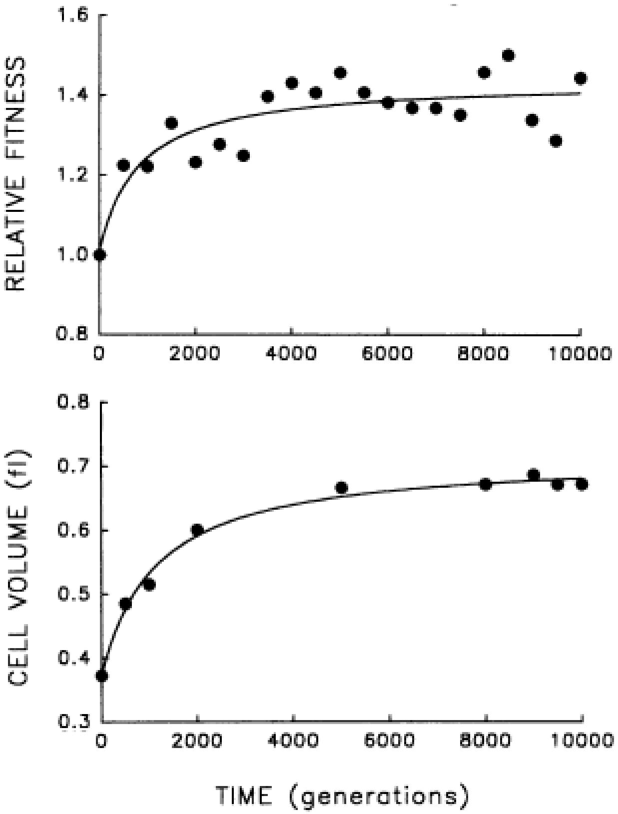

Figure 9.6. Idealized views of the response of cell growth rates to environmental effects. **A)** The black lines denote the phylogenetic relationship between the maximum rate of cellular growth, $r_{\max}$, taken from Figure 8.5, where it is shown that the scaling is positive for bacteria but negative for eukaryotes. The four black dots denote hypothetical species, and the red arrows denote the universal reduction in cell size and growth rate in response to reduced nutrient supplies. **B)** The joint response of cell size and growth rate to changes in nutrient availability and temperature for an arbitrary genotype. The slopes and end points of the lines are arbitrarily placed, although it is known that $r_{\max}$ is reduced at lower temperatures, and the overall expectation is that when nutrient concentrations are manipulated so that cells are dividing at the same rates at different temperatures, cell size will be larger at the lower temperatures.

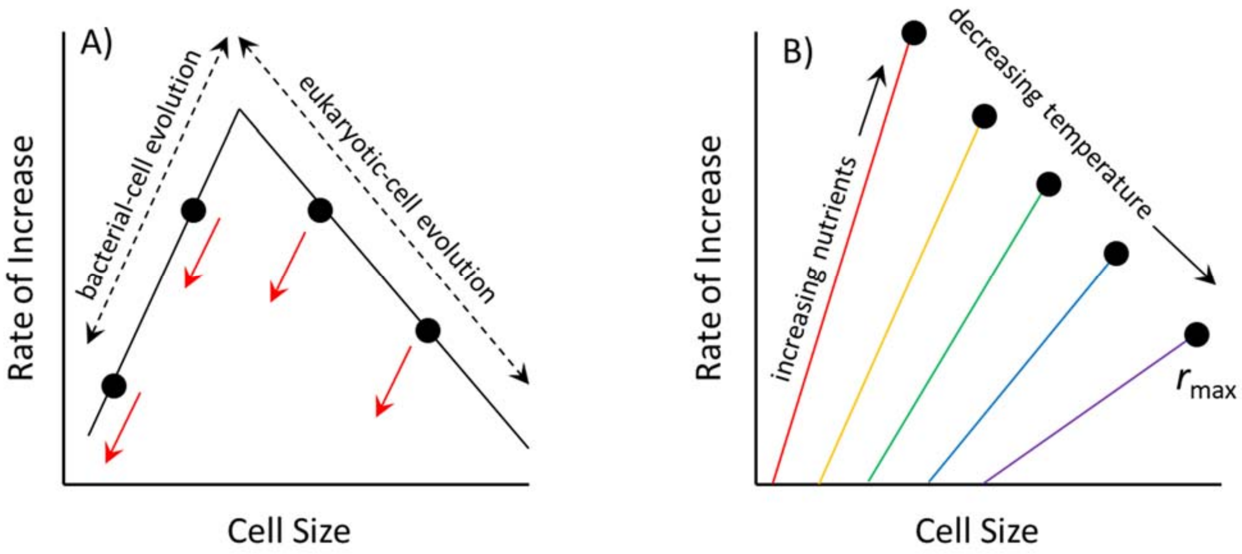

Figure 9.7. Pearson type-III distributions fitted to data on the frequency distributions of cell-division times for two species of the bacterium *Bacillus.* From Powell (1958).

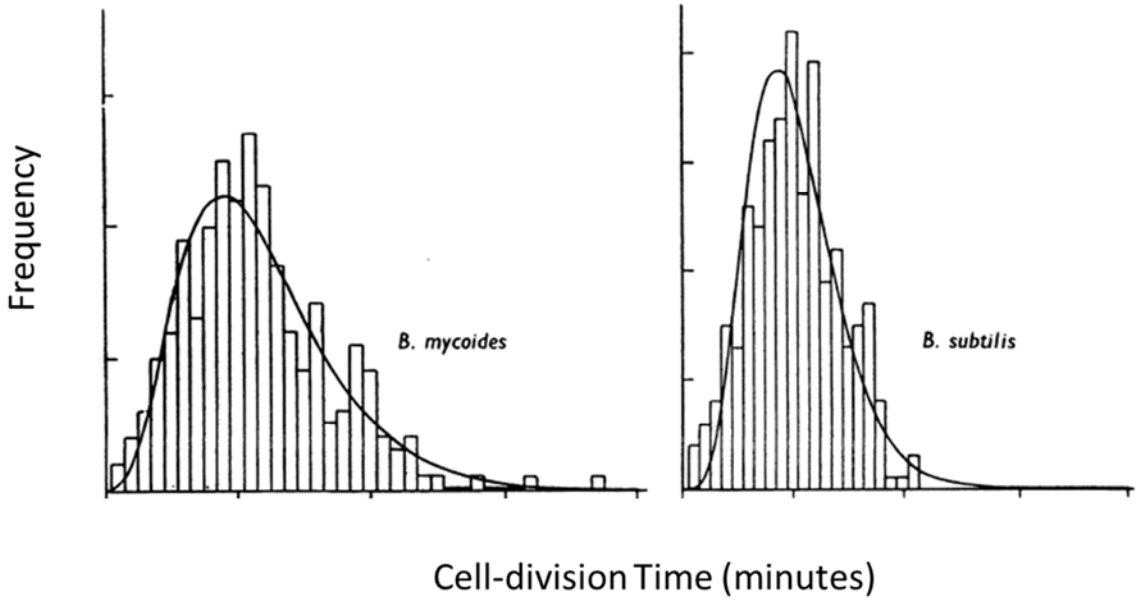

Figure 9.8. Coefficient of variation for the number of molecules inherited by daughter cells as a function of the coefficient of variation for volume of sister cells, $\mathrm{CV}(V)$. Results are given relative to the case with simple binomial sampling, as a function of the mean number expected in parent cells, $\overline{n}$, and calculated with Equation 4.9. The coefficient of variation of the number of molecules per parent cell, $\mathrm{CV}(n_0)$, is assumed to be equal to 0.1 (based on empirical estimates described in the text).

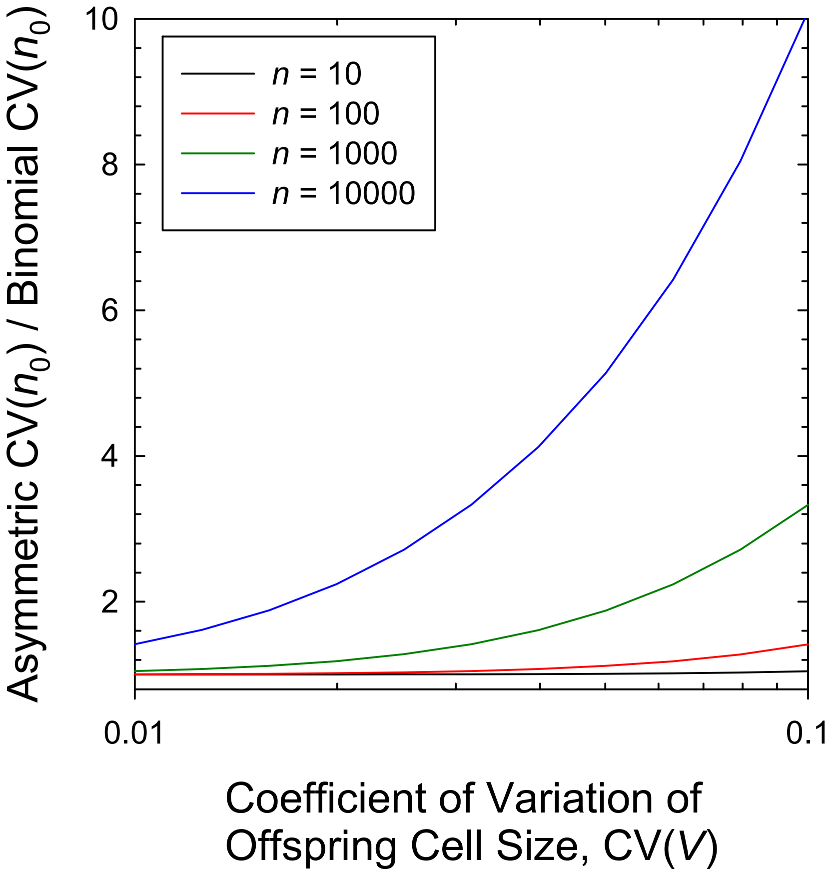

Figure 9.9. The response to directional selection for increased phenotypic values of a continuously distributed trait, represented by the transition of the black to the red bell-shaped curve. The difference between mean phenotypes after and before selection, but before reproduction, is known as the selection differential. The response to selection is determined by the degree to which offspring phenotypes resemble those of their parents, as illustrated by the diagonal dashed line, the slope of which is known as the heritability of the trait. In the absence of genetic variation, this regression line will have a slope equal to zero. Regardless of the heritability, in the absence of selection, the offspring mean phenotype is expected to equal that of the parental generation.

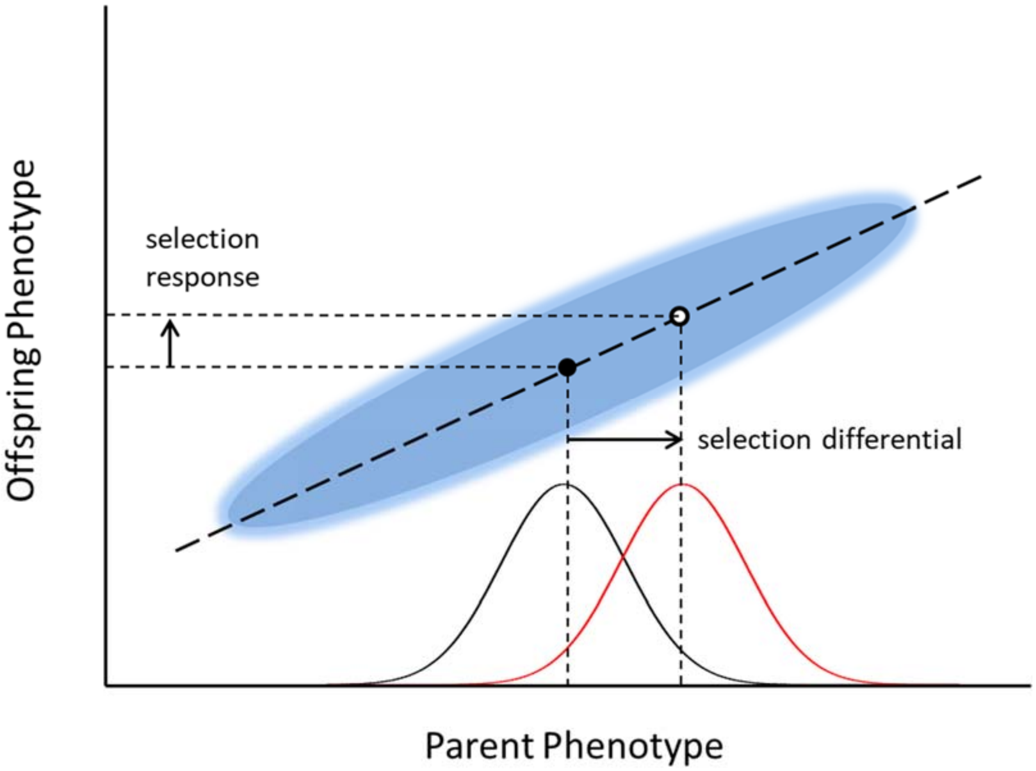

Figure 9.10. The influence of the form of the fitness function on the average fitness of a population of cells. The red lines are fitness functions denoting relationships between fitness and phenotype, and the dashed lines demarcate the expected fitnesses for three phenotypes, with the flanking two being equidistant from the one in the middle. In the absence of phenotypic variation, the mean fitness will be equal to the expectation for the middle phenotype (thick dashed lines), whereas in the presence of variation (here, assumed to be symmetrical around the mean), the average fitness for the population of cells (blue arrows) will deviate in a direction depending on the curvature of the fitness function.

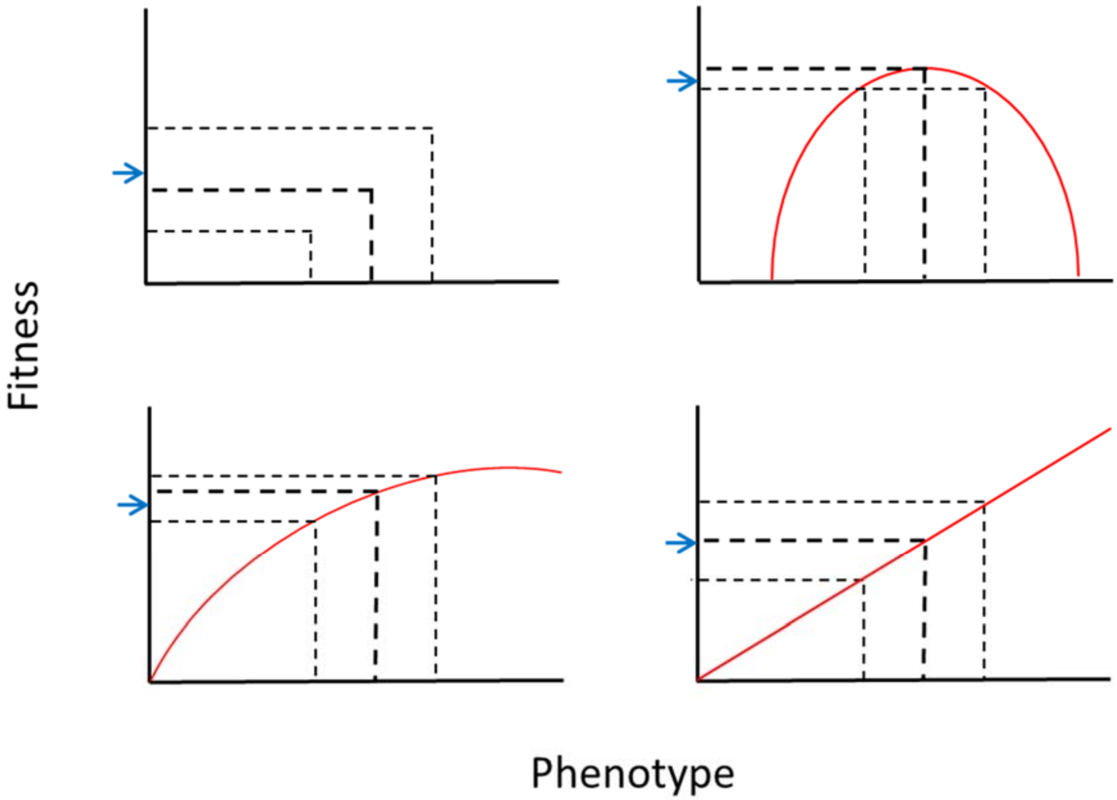

Figure 9.11. A conceptualized partitioning of cellular proteins into three general pools, one of which contributes an invariant proportion to the total pool regardless of the cellular nutritional state (after Scott et al. 2010). The total pool of ribosomal proteins is also considered to contain a small invariant fraction associated with inactive ribosomes. This leaves the pools of active ribosomal proteins and metabolic proteins free to vary with respect to each other (the green-yellow boundary associated with the double-headed arrow can move), but constrained to sum to areas under the yellow and green sectors.